

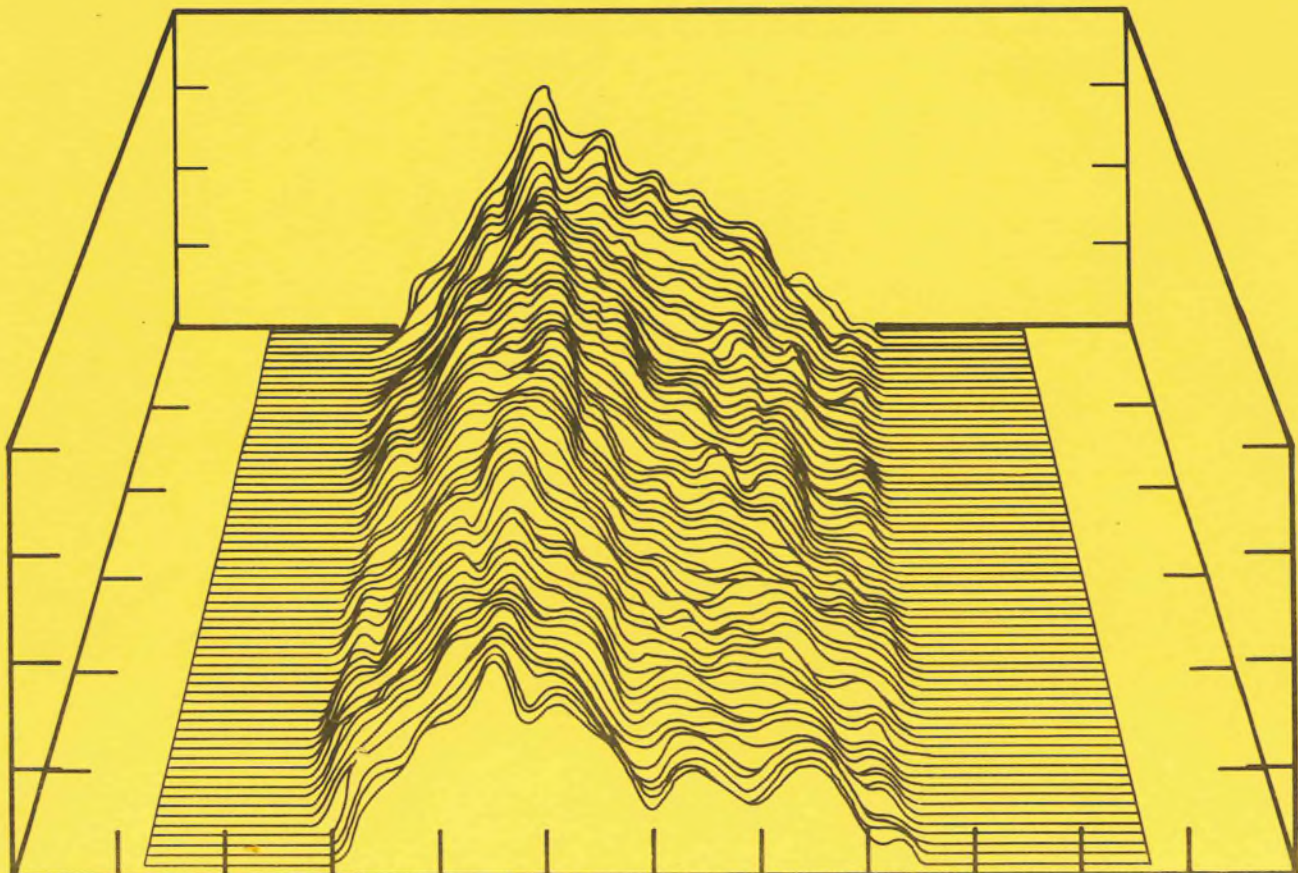
# canadian acoustics

## acoustique canadienne

APRIL, 1985 - Volume 13, Number 2

AVRIL, 1985 - Volume 13, Numéro 2

Editorial	1
Acoustics Week 85	2
Sound Propagation Over an Isolated Seamount Off the Canadian West Coast G.R. Ebbeson and N.R. Chapman	3
Acoustical Characteristics of Guns as Impulse Sources M.J.R. Lamothe and J.S. Bradley	16
Measurement of Sound Transmission Loss by Sound Intensity R.W. Guy and A. de Mey	25
Acoustical Exploration Technique for Detecting Oil Trapped Under Sea Ice H.W. Kwan and H.W. Jones	45
News	55
CSA Activities	56



# canadian acoustics

The Canadian Acoustical Association  
P.O. Box 3651, Station C  
Ottawa, Ontario K1Y 4J1

Second Class Mail Registration  
No. 4692

Undeliverable copies — return  
postage guaranteed.

Back issues (when available) may be obtained  
from the Associate Editor — Advertising  
Price \$4.00 incl. postage

CANADIAN ACOUSTICS publishes refereed articles and news items on all aspects of sound and vibration. Papers reporting new results as well as review or tutorial papers, and shorter research notes are welcomed in English or in French. Two copies of submission should be sent to either the Editor-in-Chief (English articles), or to the Editor (French articles). Complete information to authors concerning the required camera-ready copy is given in the first issue of each volume.

# acoustique canadienne

*l'Association Canadienne de l'Acoustique*  
C.P. 3651, Succursale C  
Ottawa, Ontario K1Y 4J1

*N° d'enregistrement (Poste*  
*deuxième classe) 4692.*

*Copies non délivrées: affranchissement*  
*de retour est garanti.*

*Des numéros anciens (non-épuisés) peuvent*  
*être obtenus en écrivant au Rédacteur Associé — Publicité*  
*Prix: \$4.00 (affranchissement inclus)*

*ACOUSTIQUE CANADIENNE publie des articles*  
*arbitrés et des informations sur tous les domaines du*  
*son et des vibrations. Les manuscrits seront inédits ou*  
*bien des aperçus, ainsi que des notes techniques,*  
*rédigés en français ou en anglais. Deux copies seront*  
*soumises au rédacteur en chef (articles en anglais), ou au*  
*rédacteur (articles en français). La forme et la*  
*préparation des manuscrits exigées pour reproduction*  
*se trouveront dans le premier numéro de chaque volume.*

---

## Editor-in-Chief/ Rédacteur en chef

John Bradley  
Division of Building Research  
National Research Council  
Ottawa, Ontario K1A 0R6  
(613) 993-2305

## Editor/ Rédacteur

Gilles Daigle  
Division de physique  
Conseil national de recherches  
Ottawa, Ontario K1A 0R6  
(613) 993-2840

## Associate Editors/Rédacteurs associés

### Printing and Distribution *Impression et Distribution*

Michael Stinson  
Acoustics, Division of Physics  
National Research Council  
Montreal Road  
Ottawa, Ontario K1A 0R6  
(613) 993-2840

### Advertising *Publicité*

Tim Kelsall  
Hatch Associates Ltd.  
21 St. Clair Avenue East  
Toronto, Ontario M4T 1L9  
(416) 962-6350

P. Nguyen  
Noranda Research Centre  
240 Hymus Blvd.  
Pointe-Claire, Québec H9R 1G5  
(514) 697-6640

## Production Staff/Equipe de production

Secretarial / *secrétariat*: L. Ernst

Graphic Design / *maquette*: S. Tuckett

## EDITORIAL

The trend to larger issues of CANADIAN ACOUSTICS continues, and we now have a small back-log of papers. We will continue to ensure that papers are printed promptly, while maintaining a reasonably stable journal size.

If there is not a 'P' or an 'F' on the bottom right hand corner of your mailing label, you will not receive further issues of CANADIAN ACOUSTICS. If you believe there are errors, please contact Alf Warnock at (613) 993-2305 (address on the last page of this issue).

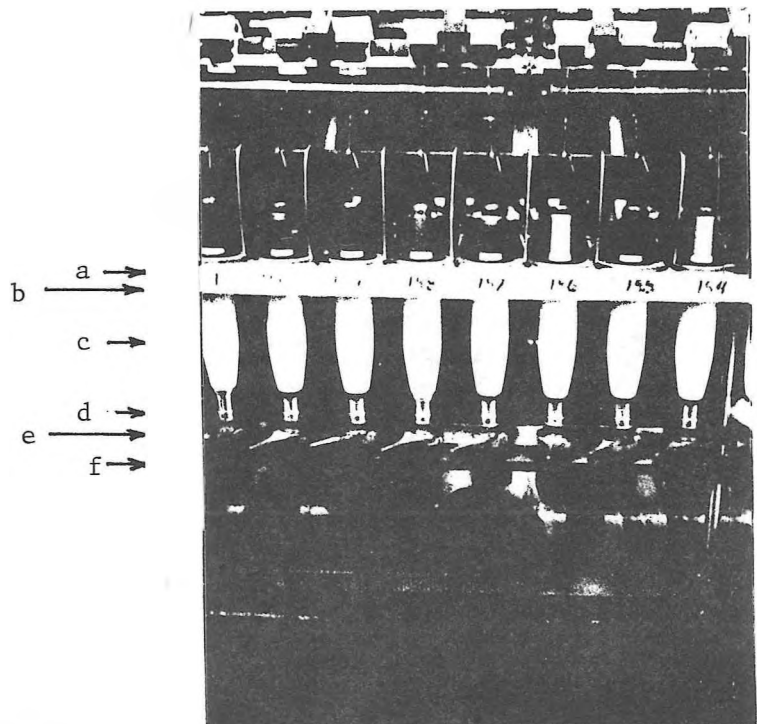
Finally, sustaining subscribers are reminded that they must be paid up before the end of May to be included on the back cover for the next four issues.

## EDITORIAL

Nous avons maintenant une accumulation d'articles à publier. Nous tâchons de les publier aussitôt que possible tout en respectant l'épaisseur de l'ACOUSTIQUE CANADIENNE.

Afin d'assurer votre abonnement à l'ACOUSTIQUE CANADIENNE, un 'P' ou un 'F' doit apparaître sur l'étiquette (en bas à droite) apposée sur votre copie. S'il y a erreur, s'adresser à Alf Warnock au (613) 993-2305.

Finalement, nous rappelons que les abonnés de soutien doivent être en règle en date du 31 mai pour figurer sur la liste en page couverture.



## CORRECTION

Nous signalons une erreur de composition volume 13, numero 1, figure 5 de l'article "Utilisation de l'intensité et de la puissance acoustique pour l'identification des sources de bruit" par G. Lemire et J. Nicolas. Une correction sur papier collant est incluse dans ce numéro afin de compléter la figure.

Figure 5. Vue d'une section du corps de la machine.  
a) anneaux, b) rail supportant les anneaux, c) bobines, d) broches (vue partielle), e) courroies d'entraînement, f) rail supportant les bobines. Poulies de tension non visibles.

Monday-Thursday, 30 September - 3 October

- "Industrial Audiometry and Hearing Conservation"  
4-day course (fee)  
Contact: Gail Edmundson, Health Sciences, Algonquin College  
(613) 725-7618

Tuesday, 1 October

- "Subjective and Objective Measurement of Loudspeakers and Criteria for Good Design"  
Seminar presented by the Division of Physics, National Research Council  
(fee)  
Contact: Dr. Floyd Toole, (613) 993-2840
- CSA Committee on Acoustics and Noise Control

Wednesday, 2 October

- "Noise Control in Buildings"  
Building Science Insight Seminar by the Division of Building Research,  
National Research Council (fee)  
Contact: B.A. Stafford, (613) 993-0646

Thursday-Friday, 4-5 October

- CAA Annual Conference  
Submission of papers on all aspects of sound and vibration are invited. A short (100-200 word) abstract is required by 1 August to ensure inclusion in the program and printing of the abstract in CANADIAN ACOUSTICS.  
Submit abstracts to: Dr. R.E. Halliwell, Division of Building Research,  
National Research Council Canada, Ottawa, K1A 0R6

Special Technical Sessions

- "Speech"  
Contact: Dr. M.J. Hunt, (613) 993-3408
- "Health Related Acoustics"  
Contact: D.A. Benwell, (613) 990-8892
- "Building Vibrations"  
Contact: Dr. J.H. Rainer, (613) 993-2305

The conference will be held at the Chimo Inn (St. Laurent Boulevard and Highway 417, Ottawa, (613) 744-1060). Attendees are encouraged to stay at this hotel to benefit from the conference rates and to reduce the cost of meeting rooms for the CAA.

The CAA Annual Business Meeting will be held on Thursday, 4 October, followed by a banquet.

# SOUND PROPAGATION OVER AN ISOLATED SEAMOUNT OFF THE CANADIAN WEST COAST

Gordon R. Ebbeson and N. Ross Chapman

Defence Research Establishment Pacific  
Forces Mail Office  
Victoria, B.C. VOS 1B0

## ABSTRACT

Acoustic shadowing, reflection, and enhancement near an isolated seamount have been studied by examining the results of an experiment carried out to measure the propagation loss over Dickins Seamount off the Canadian west coast. Two types of sound sources were used: a 230-Hz cw projector towed at depths of 18 and 184 m; and 0.82-kg explosives detonated at depths of 24 and 196 m. The receiving system had hydrophones spaced in depth from 329 to 633 m. In the acoustic shadow region, the propagation loss for the shallow sources increased by 15 dB over the loss measured in the absence of the seamount. Examination of the multipath propagation loss for the shots revealed that the received signals consisted of two arrivals. The first and dominant pulse was determined to be a diffracted wave while the subsequent group of weaker pulses was attributed to a series of bottom and surface reflections. Strong reflections from the seamount were observed when the shallow cw source was 3 to 5 km from the seamount peak. For source positions closer to the peak, these reflections changed to downslope reflections resulting in an enhancement of the directly received energy. Only minimal effects were observed in the results for the deep sources because most of the source energy propagated along the sound-channel axis above the seamount peak.

## SOMMAIRE

Une expérience, qui avait pour but de mesurer les pertes obtenues lorsqu'il y a propagation au-dessus d'un mont de Dickins, a été réalisée au large des côtes canadiennes. L'ombrage, la réflexion et l'amplification acoustique créés au voisinage d'un mont sous-marin ont été étudiés. Deux types de sources sonores ont été utilisées: un projecteur d'une fréquence de 230 Hz remorqué à des profondeurs de 18 et 184 m, ainsi que 0.82 Kg d'explosif déclenché à des profondeurs de 24 et 196 m. La réception des signaux était assurée par un groupe d'hydrophones disposés sur un axe vertical à des profondeurs variant de 329 à 633 m. Dans la région d'ombrage acoustique, les pertes de propagation sont augmentées de 15 dB comparativement aux pertes mesurées en absence de mont sous-marin. Un examen plus attentif a révélé que le signal reçu était composé de deux groupes de signaux ayant des temps d'arrivée différents. Le premier groupe reçu a été attribué à l'onde diffractée, tandis que le second groupe, constitué d'impulsions plus faibles, a été

expliqué par les réflexions sur le fond et à la surface de l'eau. De fortes réflexions, introduites par le mont sous-marin, ont été observées lorsque la source était située de 3 à 5 km du sommet. Pour des distances inférieures, ces réflexions se réorientent partiellement vers le fond pour finalement s'ajouter aux ondes suivant le parcours direct. De faibles effets ont été observés dans le cas des sources en eau profonde dû au fait que l'énergie se propage le long de l'axe situé au-dessus du sommet.

## INTRODUCTION

Acoustic propagation over an isolated seamount has been studied to determine how the seamount interacts with the propagating acoustic energy, as well as how these interactions vary with the depths of the sound source and receiver, and the position of the source with respect to the seamount and receiver.<sup>1,2</sup> A series of experiments was carried out over Dickins Seamount which is located at 54°32'N, 136°55.5'W as shown in Figure 1. Unlike previous investigations,<sup>3-9</sup> the present propagation loss measurements were made using both a 230-Hz cw source and small explosive charges at ranges relatively close to the seamount. With the detailed knowledge of the bathymetry that was available and the lack of interference from other seamounts, it was possible to perform a very detailed study of the seamount shadowing effect. These features also made it possible to extend the study to include an investigation of the reflection of the source energy from the seamount and the closely related downslope reflection enhancement.

## DESCRIPTION OF THE EXPERIMENT

The configuration of the source tracks with respect to the receiving system and Dickins Seamount is shown in Figure 2. A continuous-wave (cw) source with a frequency of 230 Hz was towed at depths of 18 and 184 m. Tracks 1 and 4 were radial runs during which the source was towed over the seamount at the shallow and deep depths, respectively, out to ranges of between 120 and 130 km. Track 2 was a radial run during which the source, towed at the shallow depth, traversed 45 km of relatively flat bottom to the east of the seamount. In addition, 0.82-kg explosives were deployed at average depths of 24 and 196 m at intervals of 1.8 km along track 5 out to a range of 130 km. The receiving system, which was at a range of 60 km (about 1.5 convergence zones) from the seamount, consisted of a vertical line array of eight omnidirectional hydrophones spaced in depth from 329 to 633 m.

The average seamount slope along the tracks was approximately 14° and the minimum depth near the peak was 420 m. A number of sound-speed profile measurements were made along the tracks of Figure 2 during the propagation experiments. The average of these profiles is shown in Figure 3. As is characteristic of this region of the Northeast Pacific, the profile has two sound channels. The upper or secondary sound channel has an axis at a depth of about 95 m while the axis of the lower or deep sound channel is near 300 m. It is important to note that the deep sound channel axis was shallower than the seamount peak.

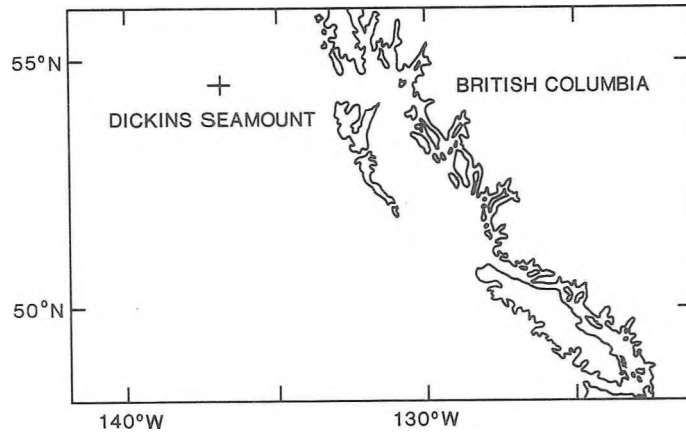


Figure 1. Location of Dickins Seamount (54°32'N, 136°55.5'W) in the Northeast Pacific Ocean.

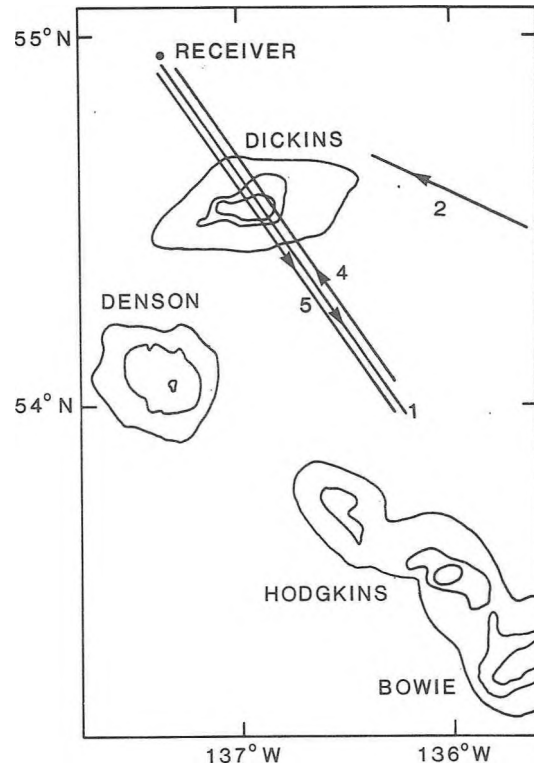


Figure 2. Orientation of the source tracks with respect to the receiver and Dickins Seamount. The depth contours are 1000, 2000, and 3000 m. For tracks 1, 2 and 4 a cw source was used while explosive charges were used for track 5.

#### ACOUSTIC SHADOWING BY THE SEAMOUNT

The geometry of these propagation loss experiments was designed so that the deep-cycling energy from the sources would, at some point along the runs, be blocked by the seamount. Although the receiver was effectively in an acoustic shadow during this blockage, some energy was still received. Ray theory predicts that the deep-cycling rays propagated over the seamount by a number of bottom-surface reflections up and then down the slope. Diffraction theory, however, predicts that the deep-cycling energy propagated over the seamount by forward scattering from the rough surface of the seamount slope and diffraction over the peak. These mechanisms are discussed in the following sections with an analysis of the measured results to determine which was the dominant source of energy in the shadow zone.

##### 1. Measurements With The CW Source

Figure 4 shows three raytracings for track 1 which were computed using the average sound-speed profile from the run and a source depth of 18 m. Each raytracing illustrates a different source position with respect to the seamount: a range from the receiver of 79 km in case A; 99 km in case B; and 119 km in case C. All bottom-bounce rays are omitted from the raytracings for clarity. For cases A and C, maximum shadowing is expected because the source is in a position which enables the seamount to intercept all of the deep refracted rays. In the absence of the seamount, these deep refracted rays

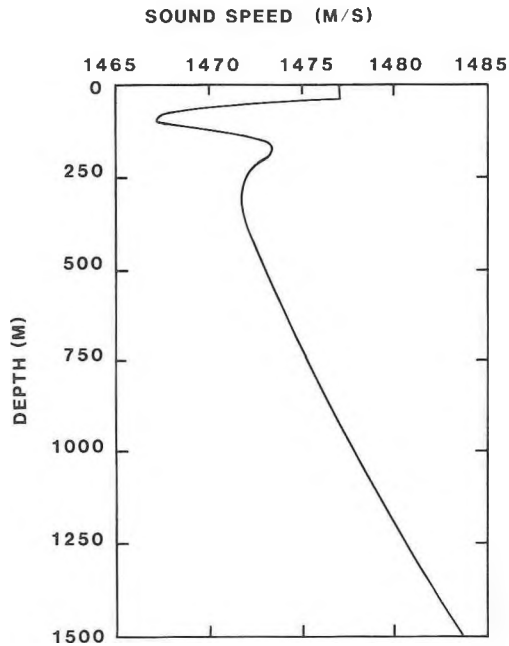


Figure 3. Average sound-speed profile from all profile measurements.

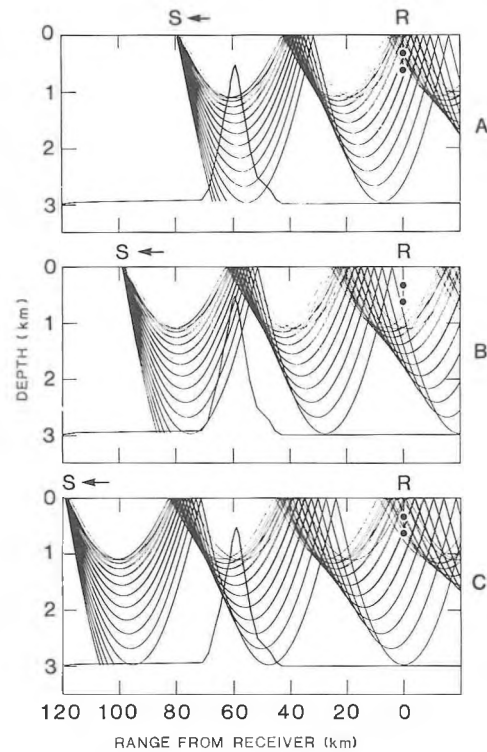


Figure 4. Raytracings for radial track 1; source depth 18 m and source angles  $-15^{\circ}$  to  $15^{\circ}$  in 1 degree increments. Receiver depths of 329 and 633 m are indicated by dots. The profile of the seamount is shown for three ranges: 79, 99, and 119 km.

would form a convergence zone at the receiver. For case B, the seamount intercepts only a small number of the deep refracted rays, so little shadowing should be seen.

Figure 5 contains the propagation loss results that were measured across the seamount (track 1) and over a flat bottom (track 2). In each case the cw source depth was 18 m, the receiver depth was 329 m, and the averaging time was 3.8 min. The smooth curve in Figure 5(a) is a propagation loss prediction from the FACT (Fast Asymptotic Coherent Transmission) ray model<sup>10</sup> with semicoherent addition. The prediction is based on the average sound-speed profile for track 1 and a flat bottom (as is assumed by FACT) with a FNWC (Fleet Numerical Weather Central) bottom loss classification type 2.<sup>10</sup> For the first 60 km, the measured results agree well with the predicted losses, particularly in the first bottom-bounce region (10-35 km) and in the first convergence zone (35-45 km). The peak (propagation loss minimum) between 57 and 60 km is an enhancement effect which is the result of acoustic reflection from the seamount and is discussed later in the paper. At ranges beyond 60 km, the point at which the source passed over the seamount, there is a marked increase in propagation loss caused by the shadowing effect of the seamount. In Figure 5(b), A, B, and C are the source ranges for the raytracings shown in Figure 4. As indicated by the raytracings, the results that were measured over the seamount (track 1) show maximum shadowing at A and C. For these ranges, the increase in propagation loss over the convergence zone level measured over the flat bottom (track 2) is about 15 dB. There is no similar increase in propagation loss at B, indicating the lack of interaction of the sound energy with the seamount.

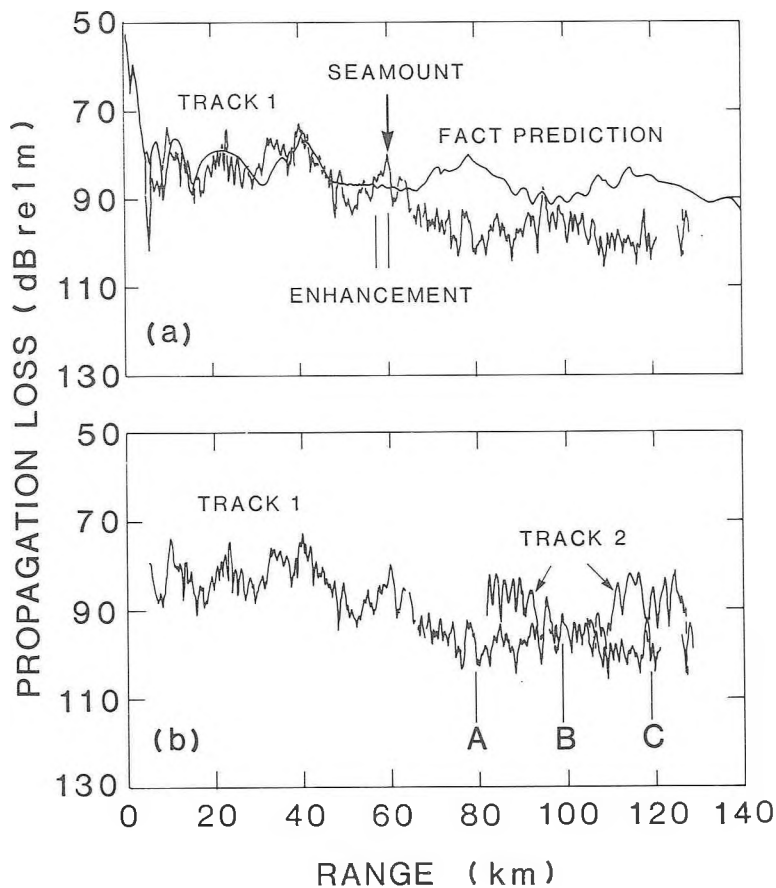


Figure 5. Measured propagation loss results for tracks 1 and 2; source depth 18 m and receiver depth 329 m. The smooth curve is a FACT model prediction based on a flat bottom. A, B, and C are the source ranges for the raytracings of Figure 4.

## 2. Ray Model Investigation Of Shadowing

The GRASS (Germinating Ray-Acoustics Simulation System) model,<sup>11</sup> which is capable of modelling range-dependent environments, was used to determine the bottom-surface propagation paths over the seamount with the cw source in positions A and C of Figure 4. These calculations used a source depth of 18 m and the average sound-speed profile and seamount bathymetry for track 1.

The investigation revealed that there are several possible ray paths over the seamount. These paths fall into one of three groups, depending upon the mode of propagation from the seamount to the receiver: (1) continuously refracted (RR) propagation; (2) refracted surface-reflected (RSR) propagation; and (3) bottom-bounce (BB) propagation. For cases A and C, the dominant arrivals at the receiver are RR arrivals which undergo one upslope reflection (1 USR) and one downslope reflection (1 DSR) on the seamount before propagating to the receiver. Secondary arrivals consist of RSR, BB and other RR arrivals with more seamount reflections. Figure 6 contains a raytracing which shows the dominant and secondary RR arrivals for case A. The dominant arrivals originate with source angles (measured from the horizontal) of  $2.8^\circ$ ,  $3.0^\circ$  and  $3.2^\circ$  while the secondary arrival has a source angle of  $4.4^\circ$ . All of the arrivals in cases A and C originate as deep refracted rays with source angles of less than  $12^\circ$ . Virtually all of the rays with greater source angles are blocked by the seamount. It was found that for each of the RR and RSR arrivals predicted by the GRASS model, the grazing angles on the seamount for the first and last reflections are both less than the  $17^\circ$  critical angle of the assumed FNWC type 2 bottom loss. Thus the model introduces zero loss at these interactions. However, for the intermediate reflections the grazing

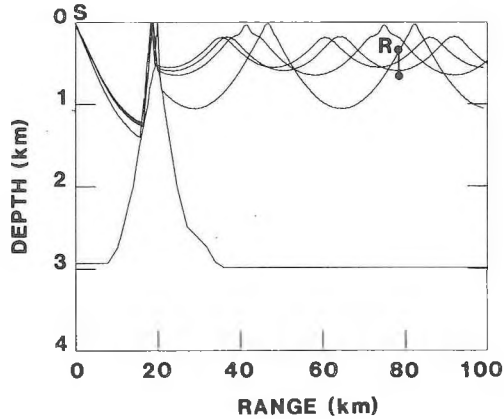


Figure 6. Raytracing showing the dominant (source angles  $2.8^\circ$ ,  $3.0^\circ$  and  $3.2^\circ$ ) and secondary (source angle  $4.4^\circ$ ) RR arrivals for track 1, case A; source depth 18 m. Receiver depths of 329 and 633 m are indicated by dots.

angles generally range from  $36^\circ$  to  $57^\circ$ , well above the critical angle, thus introducing losses in the order of 6 to 9 dB per bottom reflection. This has the effect of reducing the significance of those paths that experience more than two reflections on the seamount. However, the GRASS model predicts that for cases A and C, there is at least one significant arrival (eigenray) that propagates to the receiver in the shadow zone with minimal interaction with the seamount (1 USR and 1 DSR), thus limiting the increase in propagation loss to the 15 dB observed in Figure 5.

### 3. Measurements With The Explosive Charges

The propagation loss results for track 5 are shown in Figure 7 for the 1/3 octave bands from 12.5 to 400 Hz. The shots were detonated at a depth of 24 m and the receiver was at a depth of 363 m. The bathymetry along the track is shown at the bottom of the figure. As was seen in the cw results, the seamount shadowing effect is evident from about 65 km, where the propagation loss increases abruptly, to about 95 km and from about 105 km out to the end of the run.

An example of the multipath arrival series measured at a source range of 79 km (case A of Figure 4) is shown in Figure 8, again for the 1/3 octave bands from 12.5 to 400 Hz. The pressure-time histories plotted in this figure are typical of those observed throughout most of the primary shadowing region between 65 and 95 km. At frequencies greater than 50 Hz, there are two significant arrivals, separated by about 0.5-0.8 s. The first arrival is a sharp pulse of width about 0.3 s, and is followed by a second arrival, or group of arrivals, which slowly decrease in magnitude over about 2 s. At this range, measurement of the multipath propagation loss indicated that the loss for the dominant first arrival was 6-10 dB less than the loss for the subsequent arrivals. At frequencies lower than 50 Hz, the behavior is significantly different, as the strong first pulse is not observed.

### 4. Diffraction Theory Interpretation Of Shadowing

The first arrival observed for the shots deployed at a source range of 79 km (Figure 8) is most likely a pulse propagating over the seamount by diffraction. Following the diffracted arrival is a group of arrivals propagating over the seamount by a number of bottom-surface reflections as predicted by ray theory. This identification of the acoustic paths was

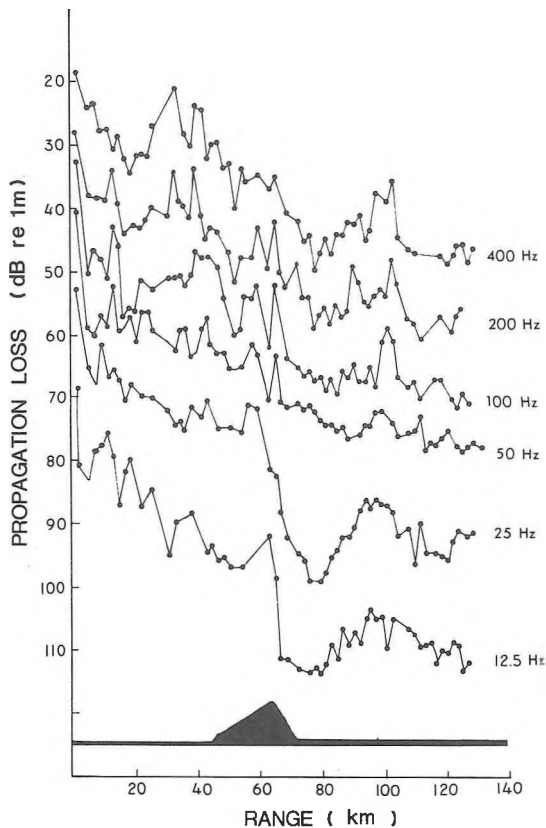


Figure 7. Propagation loss versus range from the receiver for the 24-m shots of track 5. The measurements are in 1/3-octave bands from 12.5 to 400 Hz and are offset by 10 dB. The location and shape of Dickins Seamount is shown at the bottom of the figure.

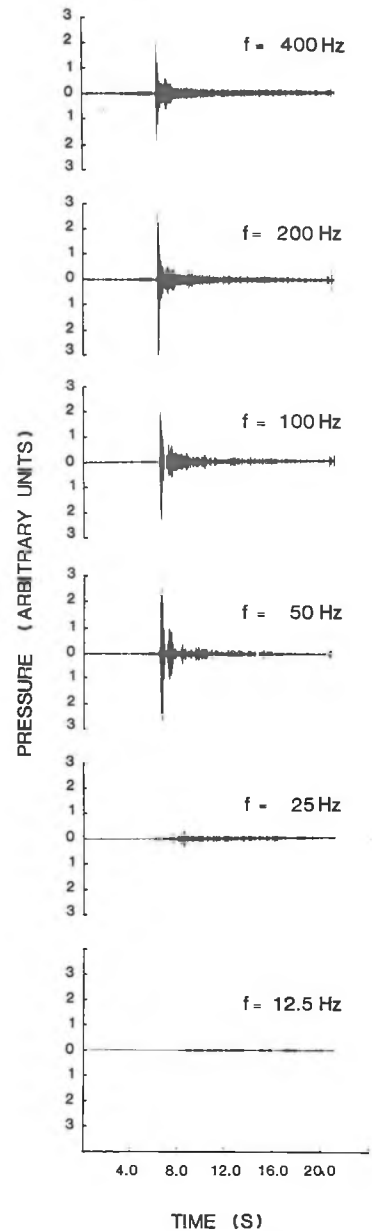


Figure 8. Pressure-time histories of a 24-m shot within the primary shadow region at a range of 79 km from the receiver along track 5. The signals have been filtered in 1/3-octave bands from 12.5 to 400 Hz.

determined by comparing the travel time of the first arrival within the shadow zone (range 79 km) with that computed by ray theory predictions with the GRASS model. The model predictions represent the earliest possible arrival times of sound propagating over the seamount by bottom-surface reflections. In the shadowing region, the ray theory predictions lagged the measured times by 0.5-1.0 s, roughly the arrival time difference observed in the data of Figure 8. A similar comparison was made at a source range of 100 km (outside the shadow zone). Here ray theory predictions coincided with the measured time since at this range the eigenrays did not interact with the seamount.

It is difficult to predict the travel time of the diffracted arrival because there is no ray-path analog for the diffraction process. However, a calculation was made for an equivalent ray path based on a model introduced by

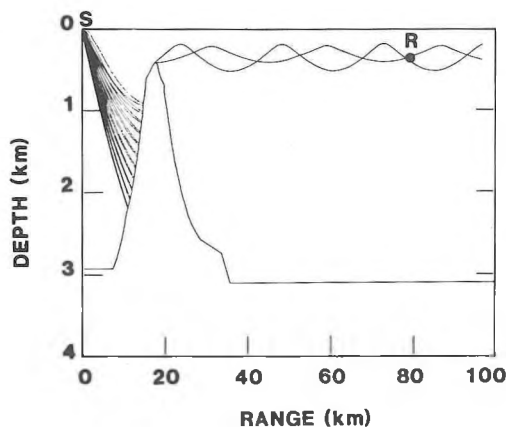


Figure 9. Raytracing showing the equivalent ray path of the diffracted wave for track 5, case A; source depth 24 m, receiver depth 363 m.

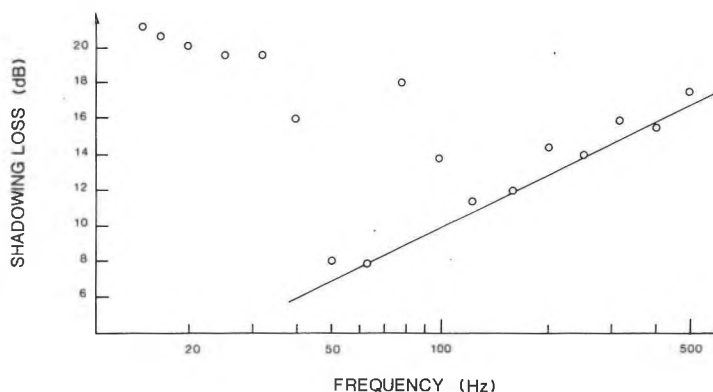


Figure 10. Shadowing loss for the track 5 24-m shots at an average range of 79 km. The solid line is a plot of the diffraction model prediction from reference 12.

Medwin et al.<sup>12</sup> The equivalent ray path of the model is shown in the raytracing of Figure 9. The model includes the theory of diffraction over a wedge and the results of laboratory experiments with a scale model of Dickins Seamount combined with a ray model of propagation. Wave theory corrections are included to model both the upslope propagation to the seamount peak by forward scattering from the rough surface of the seamount and the three-dimensional diffraction over the peak. For the travel time prediction of the diffracted arrival, ray theory was used to calculate the travel time from the source to the seamount, and from the seamount peak to the receiver. The time taken to reach the seamount peak by forward scattering up the slope was calculated using average sound-speeds over 100-m depth segments. The predicted total travel time for the range of 79 km was 54 s, in close agreement with the measured value of 53.5 s.

The shadowing loss, which is loosely defined as the increased loss caused by the interaction with the seamount over that expected in the absence of the seamount, was computed for the results of Figure 7 by subtracting the FACT model predictions for the loss over a flat bottom from the measured data. The result was the average shadowing loss as a function of frequency for the range interval 77-82 km as shown in Figure 10. Assuming that the dominant contribution is due to the diffracted arrival, the diffraction model of Medwin et al.<sup>12</sup> predicts an  $f^{1/2}$  dependence for the shadowing loss. This prediction, shown by the solid line, is in good agreement with the measured results for frequencies greater than 50 Hz, but fails to model the results obtained at lower frequencies. It is possible that the increase in shadowing loss at low frequencies is due to surface-decoupling which causes an increase in the propagation loss for shallow sources.<sup>13,14</sup> However, the disagreement at low frequencies could also be caused by a change in the scattering behavior from rough-surface forward scattering (for  $f > 50$  Hz) to smooth-surface specular reflection (for  $f < 50$  Hz). If the seamount slope is effectively smooth for low frequencies, only the arrival predicted by ray theory would propagate over the seamount. There is some support for this hypothesis in the multipath arrival histories measured in the primary shadow region. As shown in Figure 8, the strong diffracted arrival is not observed at frequencies below 50 Hz.

## ACOUSTIC REFLECTIONS FROM THE SEAMOUNT

During the propagation loss experiments, when either the shallow cw or shallow explosive sources were on the same side of the seamount as the receiver and within 15 km of the seamount peak, reflections from the seamount were found to be significant. These reflections appeared over the entire range of receiver depths (329-633 m). Ray theory predicts that the reflections were a result of the seamount redirecting the source energy through a series of bottom-surface reflections up and then down the seamount side.

### 1. Measured Reflections

Figure 11 shows a series of time-averaged spectra for the portion of track 1 when the cw source approached to within 10 km of the seamount peak. The receiver depth was 329 m and the length of each average was 3.8 min, corresponding to a range interval of 0.68 km. The direct arrival<sup>15</sup> in the spectra has a down-Doppler frequency shift because the source ship was opening range from the receiver. Because the source was closing range on the seamount, the seamount-reflected arrivals have up-Doppler shifts.

In these results, the Doppler-shifted direct arrival is dominant in level and stable in frequency throughout the 10-km range interval. Raytracings based on the average sound-speed profile and measured bathymetry of track 1 indicate that the energy of the direct arrival originated from the source at an angle of about  $16^\circ$  and propagated to the receiver via second bottom-bounce paths. The measured Doppler shift of the direct arrival, which can be related to the source angle through ship speed and the sound-speed at the source, also indicates an angle of about  $16^\circ$ . There are two reflected arrivals with

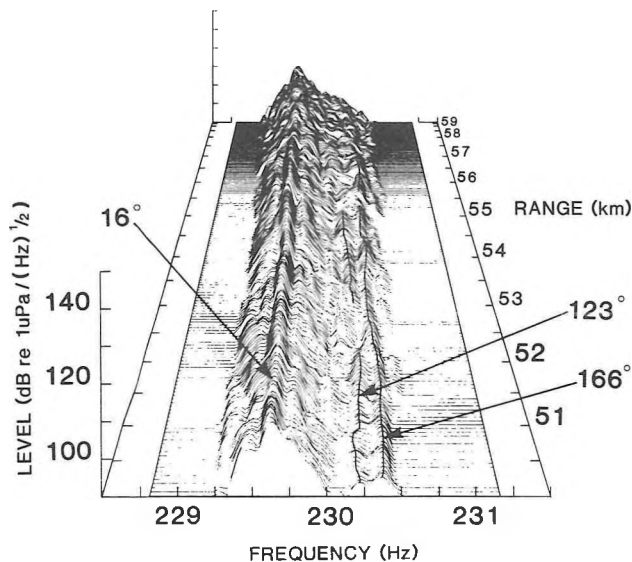


Figure 11. Variation of the measured spectral results with range for track 1; source ranges 50 to 60 km, source depth 18 m, and receiver depth 329 m. The seamount peak was at a range of 60 km. The arrival labelled  $16^\circ$  is the direct arrival while the  $123^\circ$  and  $166^\circ$  arrivals are arrivals reflected back from the seamount.

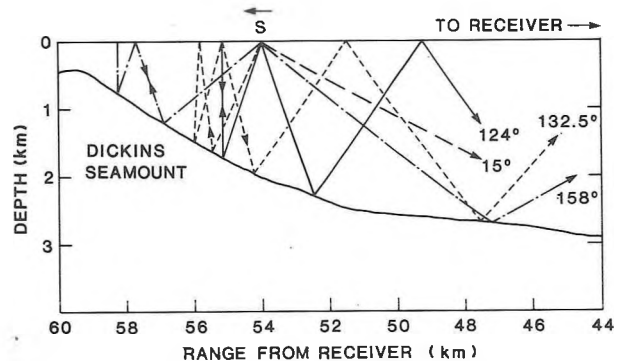


Figure 12. Raytracing illustrating the reflection process with the source 6 km from the seamount peak along track 1; source depth 18 m and source angles  $15^\circ$ ,  $124^\circ$ ,  $132.5^\circ$ , and  $158^\circ$ .

distinctly different Doppler-shifts evident in the first 5 km of the figure. Both reflected arrivals are relatively stable in frequency over that range interval and their Doppler shifts indicate that the source angles from which they originated were about  $166^\circ$  for the dominant arrival and about  $123^\circ$  for the secondary arrival. The difference in level between the dominant reflected arrival and the direct arrival averages about 14 dB over the 5-km interval with a minimum difference of 6 dB at a source range of 56 km (measured when the source was 4 km from the seamount peak).

## 2. Ray Model Investigation Of Reflection

The GRASS model was used to investigate the reflection mechanism using the same environment and geometry as that for the study of seamount shadowing. Figure 12 shows a raytracing with a source range of 54 km (6 km from the seamount peak). The angles in the figure are the source angles of the eigenrays. Of all the energy insonifying the seamount, only that energy represented by the reflected rays of this figure propagates to the receiver.

The  $158^\circ$  ray is the dominant reflected arrival. It undergoes 2 USR and 2 DSR before propagating to the receiver via a 3-BB path. The secondary arrival from  $124^\circ$  undergoes 1 USR, 2 DSR, and 4 BB before reaching the receiver. The  $15^\circ$  ray is the dominant direct arrival and undergoes 2 BB while propagating to the receiver. These three arrivals are close enough in source angle to those seen in the measured results of Figure 11 to indicate that the dominant reflected paths have been identified. Similar results were found when the ray investigation was carried out at source ranges of 53, 55, and 56 km.

## ACOUSTIC ENHANCEMENT BY THE SEAMOUNT

It was found during the propagation loss experiments that when either the shallow cw or shallow explosive sources were nearly over the seamount peak, an appreciable signal enhancement of the direct arrival was produced. This enhancement was observed over the entire range of receiver depths (329-633 m). The cw measurements indicated that during this enhancement the reflected arrival had nearly the same Doppler shift as the direct arrival. Ray theory predicts that the direct arrival was enhanced with energy that was converted via downslope reflection on the seamount to RSR paths.

### 1. Measured Enhancement

Figure 13 contains the time-averaged spectra for the last 4 km of data displayed in Figure 11. At source ranges beyond 57 km, the direct arrival in the down-Doppler region is paired with a second arrival which has a slightly smaller down-Doppler shift. The magnitude of that shift indicates that the new arrival originated from the source at an angle of about  $40^\circ$ . It appears that as the source approached to within 3 km of the seamount peak, the reflected path shifted to that of a single DSR arrival which originated with a source angle of about  $40^\circ$ . The results shown in the figure also indicate that as the source approached to within 1 km of the peak, the reflected arrival became inseparable from the direct arrival. This resulted in an enhancement of the direct arrival that was responsible for the 10-dB decrease in the propagation loss at 60 km as shown in Figure 5.

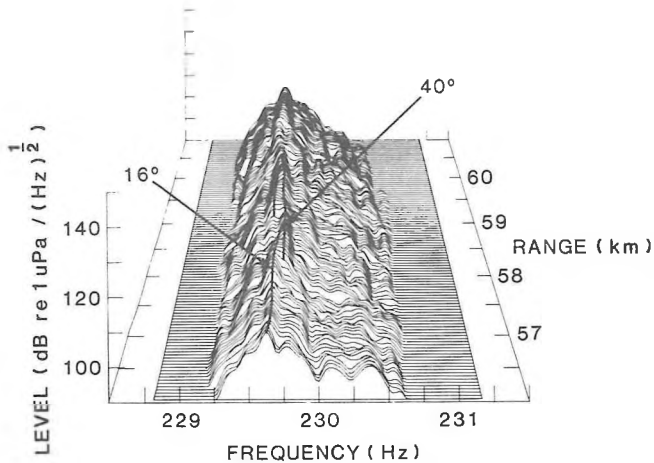


Figure 13. Variation of the measured spectral results with range for track 1; source ranges 56 to 61 km, source depth 18 m, and receiver depth 329 m. The seamount peak was at a range of 60 km. The 16° arrival is the direct, while the 40° arrival was reflected from the seamount.

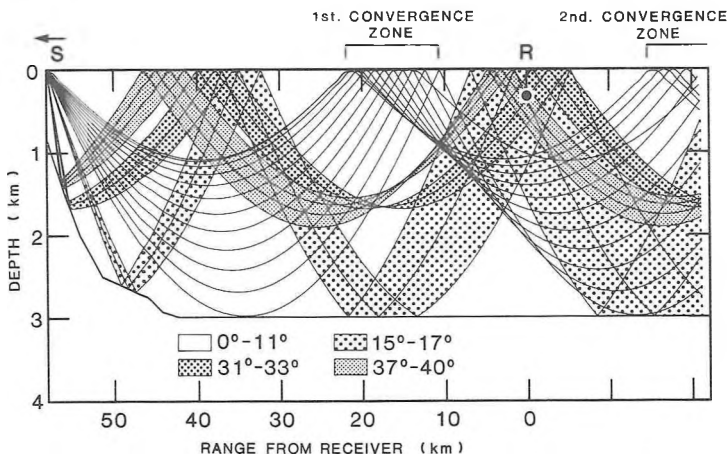


Figure 14. Raytracing illustrating the enhancement process with the source 2 km from the seamount peak along track 1; source depth 18 m, receiver depth 329 m, and source ray fans 0° to 11°, 15° to 17°, 31° to 33°, and 37° to 40° in 1 degree increments.

## 2. Ray Model Investigation Of Enhancement

The GRASS model was used to determine the mechanism which was responsible for the enhancement of the direct arrival using the same conditions as in the previous studies. Figure 14 shows a raytracing which illustrates the enhancement process at a source range of 58 km (2 km from the seamount peak). Four ray fans are plotted: the 0° to 11° fan which forms the convergence zones; the 15° to 17° fan which forms the second bottom-bounce arrival at the receiver; the 31° to 33° fan; and the 37° to 40° fan. The latter two ray fans form two convergent arrivals, each of which surface in the same region as the second bottom-bounce arrival. As the raytracing illustrates, the second bottom-bounce signal (direct arrival) is enhanced with energy that reflects (DSR) from the side of the seamount and then propagates along RSR paths to the receiver. The arrivals illustrated in this raytracing compare well in source angles with those calculated from the Doppler shifts observed in Figure 13 thus suggesting that the propagation paths of the enhancing arrivals have been correctly identified. Similar results were found when the ray investigation was carried out at source ranges of 57, 59, and 60 km. In agreement with the measured results of Figure 5, no enhancement effect is predicted for the ranges beyond 60 km, the point at which the source passes over the seamount peak.

## RESULTS FOR THE DEEP SOURCES

The propagation loss results for the deep sources indicated that the seamount did not present as significant a barrier to sound propagation as for the shallow sources. Because the energy from the deep sources was confined more closely to the sound-channel axis, most of the sound propagated over the peak without interacting with the seamount. Consequently, the shadowing effect was greatly reduced and the source energy that propagated along the channel axis masked out any of the reflected or enhancing arrivals that might have been present.

## CONCLUSIONS

These experiments have provided a reasonably detailed accounting of the acoustic interaction of low-frequency sound with Dickins Seamount, a relatively isolated bathymetric feature located off the Canadian west coast. The investigation revealed three types of acoustic interactions: shadowing; reflection; and downslope enhancement. The occurrence of these interactions and their effects on the propagation loss measured at a receiver located 60 km from the seamount were found to depend on both the depth and position of the source relative to the seamount and receiver.

When the source was shallow and in a position on the opposite side of the seamount from the receiver, such that the seamount intercepted the deep refracted energy, an acoustic shadow was cast over the receiver. Within this shadow, the propagation loss to the receiver increased by up to 15 dB over the convergence zone level measured over an area with a flat bottom. An examination of the multipath propagation loss results revealed that the source energy received in the shadow zone was composed of two arrivals. The first and dominant arrival resulted from deep refracted energy that was forward-scattered by the rough surface of the seamount slope and then diffracted over the peak. This was followed by a group of secondary arrivals composed of deep refracted energy that propagated over the seamount by a number of bottom-surface reflections up and then down the slope. However, for frequencies less than 50 Hz, only the reflected arrivals were observed. It is speculated that this was caused by a change in the scattering mechanism from rough-surface forward scattering at high frequencies to smooth-surface specular reflection at low frequencies. These results are supported by a diffraction model of seamount shadowing introduced by Medwin et al.<sup>12</sup>

When the shallow cw source approached the seamount to within 10 km from the same side as the receiver, acoustic energy was reflected from the seamount back to the receiver. Because of the Doppler shift created by the moving source, these reflections were separable in frequency from the directly received energy. A ray model investigation indicated that the reflections were the result of the seamount redirecting the source energy through a series of bottom-surface reflections up and then down the seamount side. It was found that the number of reflections required to turn the energy was a function of the angle at which the energy left the source. At closer ranges, when the source was within 3 km of the seamount peak, a portion of the source energy underwent a single downslope reflection from the seamount slope before being launched onto an RSR path to the receiver. Because this reflected arrival had essentially the same Doppler shift as the directly received energy, it was inseparable from it, and an enhancement of the direct arrival at the receiver resulted.

## REFERENCES

1. G.R. Ebbeson and R.G. Turner, "Sound Propagation Over Dickins Seamount in the Northeast Pacific Ocean", J. Acoust. Soc. Am. 73, 143-152 (1983).
2. N.R. Chapman and G.R. Ebbeson, "Acoustic Shadowing by an Isolated Seamount", J. Acoust. Soc. Am. 73, 1979-1984 (1983).
3. J. Northrop, "Underwater Sound Propagation Across the Hawaiian Arch", J. Acoust. Soc. Am. 48, 417-418 (1970).
4. R.W. Bannister, D.G. Browning, and R.N. Denham, "The Effect of Seamounts on SOFAR Channel Propagation", J. Acoust. Soc. Am. 55, 417 (1974).
5. G.B. Morris, "Preliminary Results on Seamount and Continental Slope Reflection Enhancement of Shipping Noise", Marine Physical Laboratory Report No. U-57/75, Scripps Institution of Oceanography, San Diego, CA (November 1975).
6. R.W. Bannister, R.N. Denham, K.M. Guthrie, and D.G. Browning, "Project TASMAN TWO: Low-frequency Propagation Measurements in the South Tasman Sea", J. Acoust. Soc. Am. 62, 847-859 (1977).
7. D.A. Nuttle and A.N. Guthrie, "Acoustic Shadowing by Seamounts", J. Acoust. Soc. Am. 66, 1813-1817 (1979).
8. K.M. Guthrie, R.N. Denham, R.W. Bannister, and D.G. Browning, "Models for Acoustic Propagation over a Seamount of the Louisville Ridge", J. Acoust. Soc. Am. Suppl. 1 69, S58 (1981).
9. R.N. Denham, R.W. Bannister, K.M. Guthrie, and D.G. Browning, "Low-frequency Sound Propagation in the South Fiji Basin", J. Acoust. Soc. Am. 75, 406-412 (1984).
10. C.W. Spofford, "The FACT Model", Vol. I, Maury Center Report No. 109, Acoustic Environmental Support Detachment, Office of Naval Research, Arlington, VA (November 1974).
11. J.J. Cornyn, "GRASS: A Digital-Computer Ray-Tracing and Transmission-Loss-Prediction System, Volume 1 - Overall Description", Naval Research Laboratory Report No. 7621, Washington, DC (December 1973).
12. H. Medwin, E. Childs, E.A. Jordan and R.A. Spaulding, "Sound Scatter and Shadowing at a Seamount: Hybrid Physical Solutions in Two and Three Dimensions", J. Acoust. Soc. Am. 75, 1478-1490 (1984).
13. R.W. Bannister and M.A. Pedersen, "Low Frequency Surface Interference Effects in Long Range Sound Propagation", J. Acoust. Soc. Am. 69, 76-83 (1981).
14. F.B. Jensen, "Sound Propagation over a Seamount", presented at the 11th, International Conference on Acoustics (I.C.A.), Paris, France, July 1983.
15. In the context of this paper, a direct arrival is any arrival which reaches the receiver without interacting with the seamount.

## ACOUSTICAL CHARACTERISTICS OF GUNS AS IMPULSE SOURCES

M.J.R. Lamothe and J.S. Bradley  
Division of Building Research  
National Research Council Canada  
Ottawa, Ontario, Canada K1A 0R6

### SUMMARY

The acoustical characteristics of five guns, including three calibres and two gun types, were measured to determine their suitability as impulse sources. Comparisons were made with spark and loudspeaker impulse sources. One 0.38 calibre revolver was found to be a suitably repeatable, omni-directional impulse source providing adequate sound energy in the octave bands from 125 to 5000 Hz.

### SOMMAIRE

Les caractéristiques acoustiques de cinq pistolets, y compris trois calibres différents et deux modèles différents, ont été mesurées pour déterminer leur aptitude à agir comme source d'impulsions. Des comparaisons ont été effectuées avec l'étincelle et le haut-parleur comme sources d'impulsions. Un revolver de calibre .38 s'est avéré être une source d'impulsions omnidirectionnelle, suffisamment reproductible, assurant une énergie sonore adéquate dans les bandes de fréquences 125-5000 Hz.

### INTRODUCTION

Impulsive sources are frequently required in both architectural and building acoustics measurements. For many years various guns have been used as impulse sources, usually to obtain reverberation times or to examine the details of reflection sequences in a room. They are potentially useful as a sound source to measure newer acoustical measures such as early-to-late arriving sound ratios, and can also be used to measure the sound transmission loss of walls.<sup>1</sup> Some authors have criticized the use of guns as impulse sources, suggesting that they are not adequately repeatable.<sup>2,3</sup> There is little published information describing the acoustical characteristics of guns. This report is intended to provide some details of their acoustical characteristics so that others can more satisfactorily decide on the suitability of this potentially very convenient impulsive source.

In this report, the characteristics of five guns are compared, including three calibres and two types of guns. The second section of the report compares the characteristics of the guns to those of sparks and loudspeakers.

### CHARACTERISTICS OF AN IDEAL IMPULSE SOURCE

There are a number of practical and acoustical characteristics of an ideal acoustical impulse source. As most measurements are made in the field, it is desirable that the source be portable and therefore light-weight. Acoustically the

source should be omni-directional and should have a smooth if not flat, broad frequency response spectrum. In addition the source must provide a large signal-to-noise ratio, and be repeatable. Room acoustic measurements are typically made in standard octave bands from 125 to 8000 Hz. Thus the source must produce significant energy over this entire frequency range, so that it is possible to obtain a minimum of 30 or 40 dB of decay before the background noise level is reached in each octave band. It is desirable that the source have at least a smooth spectrum so that results can later be corrected for the non-uniform source frequency response spectrum. The requirement for a broad source spectrum normally coincides with having a very short duration impulse that would permit the identification of individual reflections. Some lack of repeatability can be overcome by averaging the responses to several pulses, but measures such as reverberation times and early-to-late sound ratios are reasonably independent of small variations in the source pulse. The directionality of the source is critical for comparison with both other measurements and calculations involving a point source because it is not possible to correct for directional source effects after measurements have been made.

Mathematically the impulse response of a linear system is exactly equivalent to the steady state response of the same system and completely describes the response between two points. Such an impulse response can be obtained directly using an impulsive source or can be calculated from the steady state transfer function between the two points.<sup>3,4</sup> This latter approach requires considerable additional signal processing calculations to produce the long impulse responses required in rooms and is not considered in this report. To directly produce impulse responses commonly used sources have included: guns, sparks, exploding balloons, and loudspeakers.

#### ACOUSTICAL CHARACTERISTICS OF GUNS

The guns tested in this study are shown in Figure 1, and included 0.22 and 0.32 calibre starter's pistols, a 0.32 calibre H & R (Harrington and Richardson) starter's revolver, and two 0.38 calibre Smith and Wesson revolvers (#1 and #2). The 0.38 calibre revolvers were modified so that the barrel was plugged and a wedge shaped piece was placed in front of the shortened cylinder. The 0.32 calibre H & R starter's revolver was of a similar construction to the modified 0.38 calibre guns. On the 0.22 and 0.32 calibre starter's pistols the exploding charge exited freely upwards from the gun and did not encounter wedges or other objects that would deflect the blast.

The gun shots were tape recorded in an anechoic room using a 1/4-inch Bruel & Kjaer condenser microphone and a Technics digital tape recorder. Each gun was recorded at a distance of 2 m and at incident angles of 0 to 180 degrees in 45 degree steps in both the horizontal and vertical planes, and four repeats were recorded for each condition after some experimentation with greater numbers of shots. Zero degrees corresponded to the gun pointing at the microphone. The recorded shots were digitized and processed by computer using a Fast Fourier Transform procedure to synthesize comparable octave band results for each gun. The 0.38 calibre guns fired black powder blanks made by Dynamit Nobel while the other guns fired smokeless Remington blanks.

Figure 2 compares octave spectra for three gun calibres for a 0 degree angle of incidence (that is the gun was pointing at the microphone). The 0.32 calibre gun has a similar spectrum shape to the 0.22 calibre gun but with greater sound energy in each octave. The 0.38 calibre gun (#1) has a much flatter spectrum with relatively much more low frequency energy than the other guns. (0.38 calibre gun results refer to the #1 gun unless the #2 gun is specified). The flatter spectrum of the 0.38 calibre gun is probably due to both the larger charge of the 0.38 calibre blank and to the slower burning black powder that was used in the blank cartridges for this gun. Although the smaller calibre guns lack sufficient energy in the lowest band (125 Hz), the 0.38

calibre gun results indicate that there is satisfactory acoustical energy in all seven octave bands.



Figure 1. Photographs of the guns: (a) 0.22 and 0.32 starter's pistols; (b) 0.32 calibre H & R revolver; (c) 0.38 calibre revolver #1; (d) 0.38 calibre revolver #2.

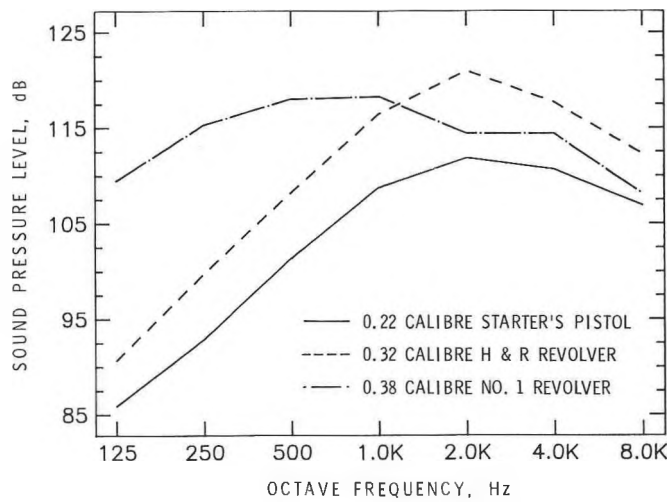


Figure 2. Octave band spectra of guns at 0 degrees incidence.

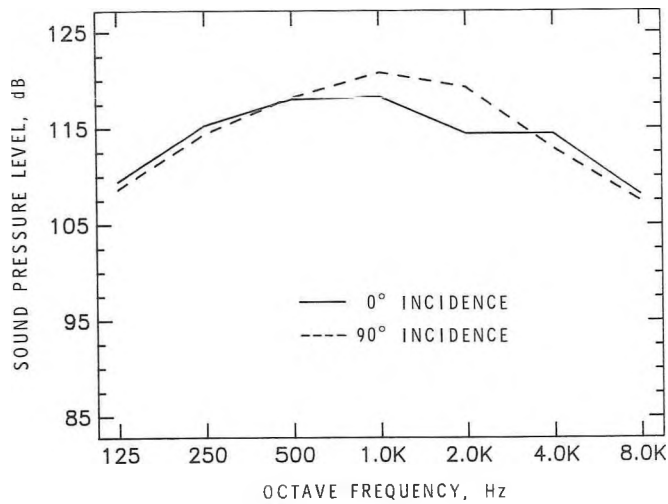


Figure 3. Octave band spectra of 0.38 calibre No. 1 revolver in horizontal plane.

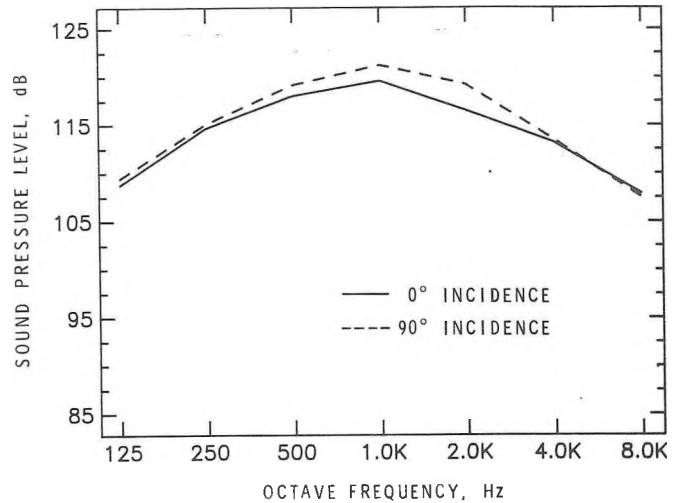


Figure 4. Octave band spectra of 0.38 calibre No. 1 revolver in vertical plane.

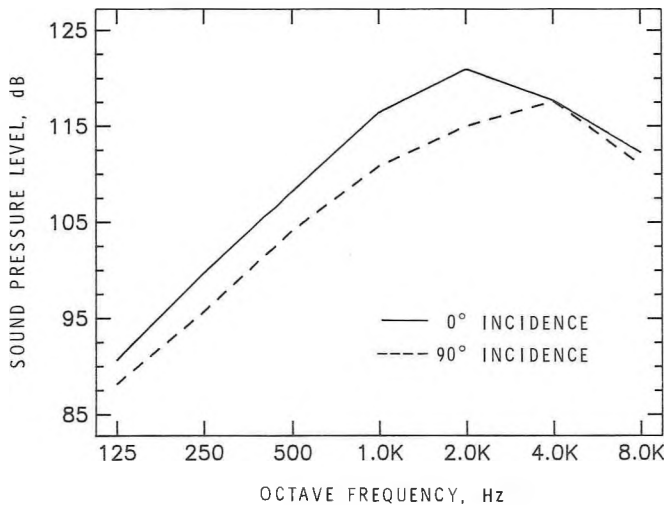


Figure 5. Octave band spectra of 0.32 calibre H & R revolver in the horizontal plane.

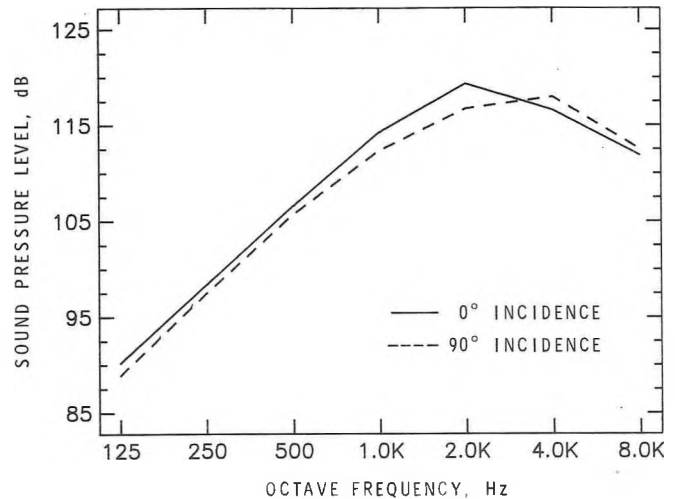


Figure 6. Octave band spectra of 0.32 calibre H & R revolver in the vertical plane.

Figures 3 and 4 show octave band spectra for the 0.38 calibre gun at 0 and 90 degree angles of incidence in the horizontal and vertical (with the gun pointing up) planes respectively. For these angles of incidence, the resulting sound levels are quite independent of angle except for small changes at 1000 and 2000 Hz. Figures 5 and 6 give similar results for the 0.32 calibre H & R gun. Figure 5 shows that for this gun sound levels for frequencies from 125 to 2000 Hz are all lower for the 90 degree incidence case than for the 0 degree case. Thus at intermediate and lower frequencies more energy is projected forward than to the side when this gun is aimed horizontally. In the vertical plane the gun is quite omni-directional.

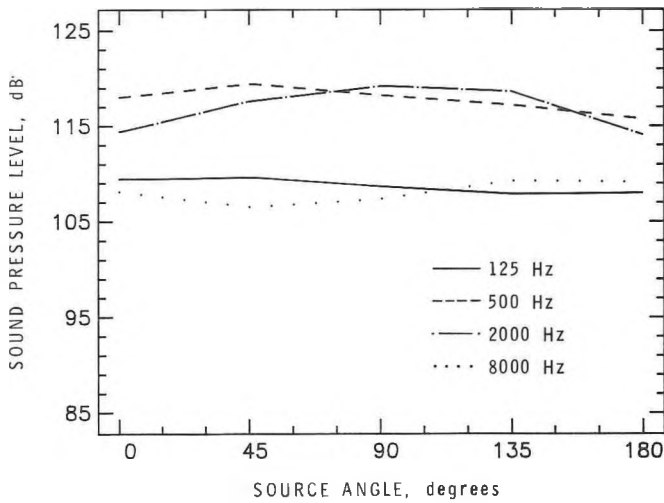


Figure 7. Octave band sound levels versus angle in the horizontal plane for the 0.38 calibre No. 1 revolver.

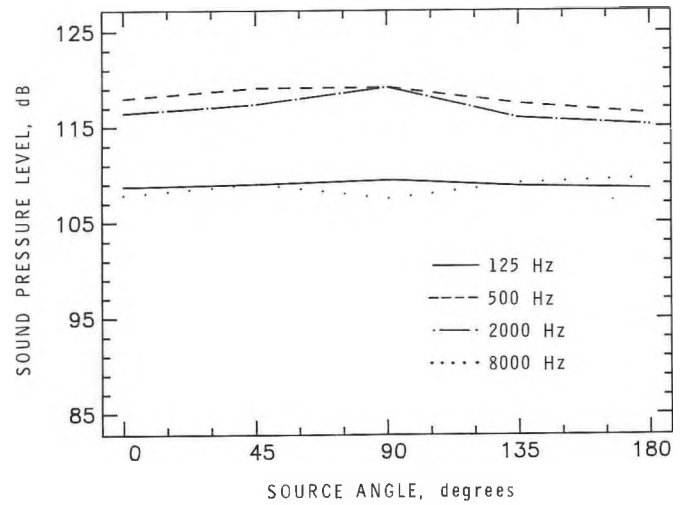


Figure 8. Octave band spectra levels versus angle in the vertical plane for the 0.38 calibre No. 1 revolver.

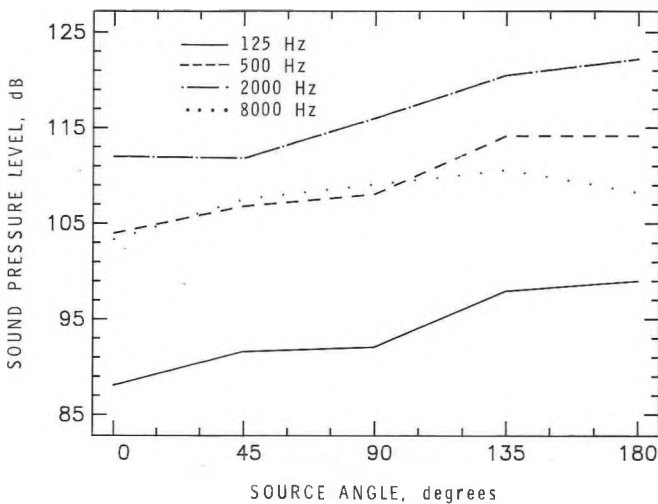


Figure 9. Octave band sound levels versus angle in the vertical plane for the 0.32 calibre starter's pistol.

Figures 7 and 8 give more complete directional information for the 0.38 calibre gun in four of the seven octave bands. These results again show that this gun is a reasonably omni-directional source at all frequencies tested. There is only a small tendency to radiate a little more strongly to the side at 1000 and 2000 Hz. The degree of omni-directionality at 8000 Hz is quite remarkable and would not be possible with other commonly used sources such as loudspeakers. The directional properties of the 0.22 and 0.32 calibre starter's pistols when rotated in the vertical plane (gun pointing up) were characteristically different. Figure 9 shows the variation in four octave bands in the vertical plane for the 0.32 calibre starter's pistol. When the gun was positioned at 180 degrees the opening in the top of the gun was pointing directly at the microphone and levels in all bands were clearly higher. Even though it was very small, this type of explosive source emitting into free space is directional and particularly so at the lowest octave band measured. This characteristic directionality indicates that one would prefer not to use this type of

gun as an acoustical source, and also helps to explain the directional properties of the other guns.

Table I summarizes the directional properties of all five guns. For each gun the range of measured sound levels is given over the ten different directional measurements in each octave band. Thus for the 0.22 calibre gun at 125 Hz the difference between the lowest and highest sound levels measured over all ten different angles of incidence was 10.3 dB. The 0.22 and 0.32 calibre starter's pistols have ranges as large as about 11 dB mostly due to the directional properties of these guns in the vertical plane. The 0.38 calibre gun (#1) has ranges from 1.8 to 5.2 dB and is thus the least directional of the five guns. In the 125 and 4000 Hz octave bands it is omni-directional within less than 1 dB and in the worst case (2000 Hz) within  $\pm 2.6$  dB.

TABLE I

Maximum Range of Measured Octave Band Levels Over All Angles

Octave	0.22 Calibre Pistol	0.32 Calibre Pistol	0.32 Calibre Revolver	0.38 Calibre #1 Revolver	0.38 Calibre #2 Revolver
125	10.3	10.9	4.1	1.8	5.4
250	10.4	9.8	4.2	2.5	5.0
500	11.5	10.2	4.6	3.7	4.9
1000	10.7	9.2	5.7	4.7	5.7
2000	9.5	10.4	6.1	5.2	6.4
4000	5.6	7.9	5.3	1.9	2.0
8000	7.5	7.3	3.1	3.1	2.2

It remains to explain the increased directionality of the very similar 0.38 calibre gun (#2) and the 0.32 H & R gun. From the 0.22 and 0.32 calibre starter's pistol results an explosive source emitting into free space was quite directional at intermediate and low frequencies. On the other guns the explosion is deflected by wedge-shaped pieces. This wedge was quite blunt and only 0.5 cm long on the 0.38 calibre (#1) gun but 1.5 cm or longer on the other 0.38 calibre gun and on the 0.32 calibre gun. It seems that the shorter blunter wedge more effectively deflects the forward-going acoustic energy to the side. Accordingly the second 0.38 calibre gun and the 0.32 calibre H & R gun are more directional when rotated in a horizontal plane.

For each set of four shots the mean sound level was calculated and the standard error of the mean was calculated in each octave band. As these standard errors varied unsystematically with varied orientation of the gun and the octave band, only the overall mean of the standard errors along with the minimum and maximum for each gun are given in Table II. The 0.38 calibre guns were similar and more satisfactory with the smaller standard errors, indicating that most of the time the mean octave band results would repeat within less than  $\pm 0.5$  dB and in the worst cases within less than  $\pm 1$  dB. The similarity between the two 0.38 calibre guns and between the two 0.32 calibre guns suggests that this repeatability is largely a function of the blank cartridges used. The 0.22 calibre gun was the most variable with a mean standard error of 0.7 dB. There is a trend for smaller calibre blank cartridges to lead to greater variability.

TABLE II

Mean, Minimum, and Maximum Standard Error of Measured Octave Band Sound Levels for Sets of Four Shots

	0.22 Calibre Pistol	0.32 Calibre Pistol	0.32 Calibre Revolver	0.38 Calibre #1 Revolver	0.38 Calibre #2 Revolver
Minimum	0.25	0.0	0.08	0.13	0.13
Mean	0.68	0.44	0.46	0.37	0.37
Maximum	1.41	1.68	0.92	0.89	0.75

### COMPARISONS WITH OTHER SOURCES

High voltage spark sources are also commonly used to create acoustical impulses. Figure 10 compares the octave spectrum of the 0.38 calibre gun with a typical spark source from Reference 2. Although the spark spectrum is quite broad, the energy is centred at 4000 Hz and there is not enough energy in the 125 Hz octave band. Some simple experiments using a borrowed high voltage source indicated that a spark source was generally quite omni-directional and that the repeatability was similar to the 0.38 calibre gun. The high voltage sources required to produce sparks are usually quite heavy and certainly not as portable as a small gun. The spark source is thus seen to be less satisfactory for architectural acoustic measurements because it lacks sufficient low frequency energy, it is not as portable, and there is added danger and inconvenience associated with the high voltage supply. The directionality and repeatability of the spark source is generally similar to that of the 0.38 calibre gun, and it may be quite useful in acoustical models where higher frequency energy is required.

Loudspeakers are also frequently used to produce impulses in rooms. In some cases measurements are made over a limited frequency range<sup>5</sup> where the response of the loudspeaker is adequately flat and omni-directional; in other cases<sup>6</sup> specially shaped pulses are fed to the loudspeaker that have been adjusted to compensate for the non-flat response of the loudspeaker. Unfortunately the directional characteristics of the loudspeaker are frequently ignored. Figure 11 plots the radiated sound level

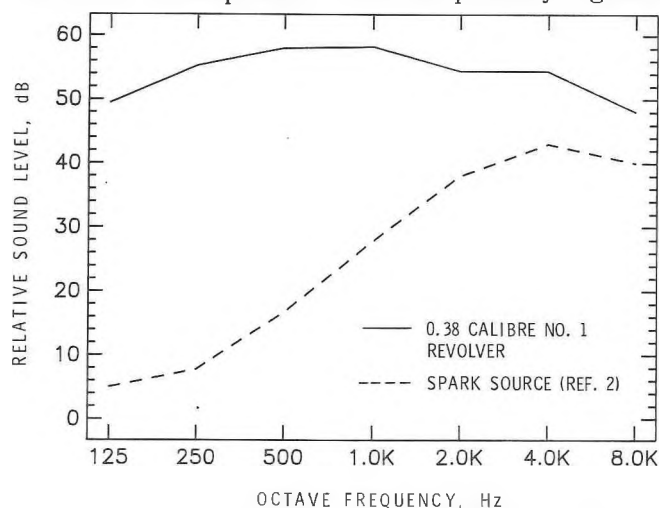


Figure 10. Comparison of octave band gun and spark source.

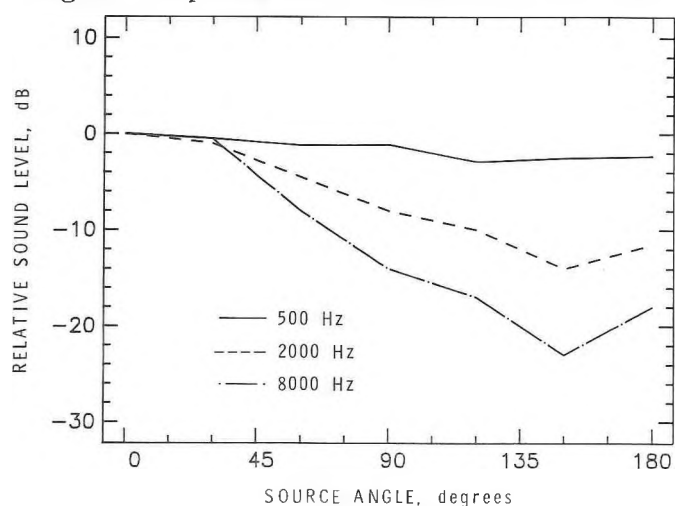


Figure 11. Octave band sound levels versus angle for a small loudspeaker.

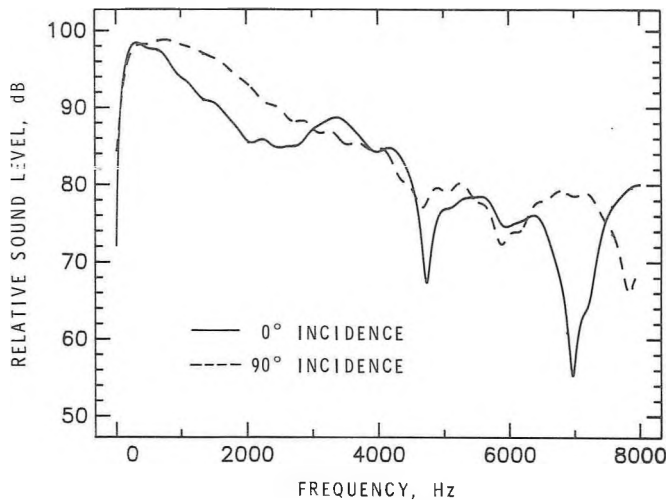


Figure 12. Narrow band power spectrum of 0.38 calibre No. 1 revolver.

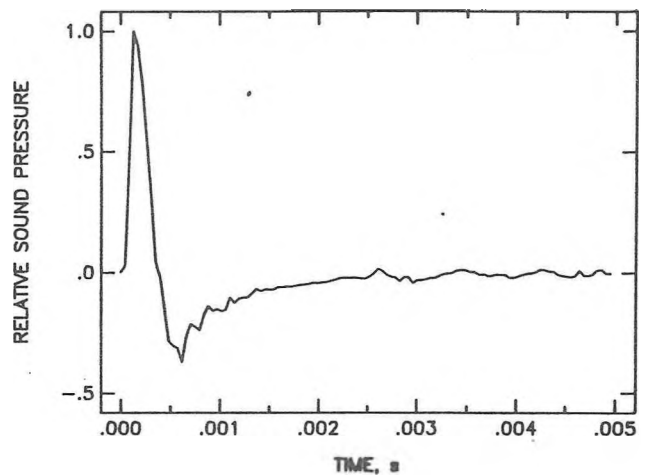


Figure 13. Anechoic time history of 0.38 calibre gun.

versus angle at three different frequencies for a small PSB Alpha-II loudspeaker. (This loudspeaker contains a 9 cm and a 2.5 cm diameter driver in a box that is approximately 12 by 22.5 by 12.5 cm). Because of its small size this loudspeaker is quite omni-directional at 500 Hz, but even at 2000 Hz it is more directional than the 0.38 calibre gun shown in Figures 7 and 8. At higher frequencies the loudspeaker becomes more directional until at 8000 Hz the radiated sound level varies by up to 23 dB with varied angle. At the same time this loudspeaker is not large enough to radiate adequate energy in the 125 Hz octave band. Although high quality loudspeakers are designed to have a flat frequency response at particular angles, the higher frequency response usually becomes quite irregular in detail. Figure 12 shows narrow band spectra of the 0.38 calibre gun for 0 and 90 degrees incidence. The spectra are quite smooth up to well in excess of 4000 Hz and so it is readily possible to correct for the non-uniform frequency response of the gun should this be necessary. In a number of ways loudspeakers are inferior to guns as acoustical impulse sources. Although they offer more precise repeatability, they and the associated electronics are much less portable. There seems to be no one loudspeaker that is small enough to be adequately omni-directional yet capable of radiating adequate power at lower frequencies. One can, at some cost, attempt to correct for the non-uniform response of a loudspeaker at one particular angle but it is not possible to correct for the very directional properties of loudspeakers.

It is sometimes of interest to have details of the time history of the source pulses, such as when attempting to identify individual reflections. Figure 13 gives an example anechoic response of the 0.38 calibre gun showing that the first zero crossing occurs after approximately 0.32 msec. The 0.32 calibre guns had shorter pulses of approximately 0.13 msec duration while the 0.22 calibre gun produced an approximately 0.18 msec pulse duration. Sparks may produce even shorter pulses which might be an advantage in some situations, but this will necessarily be associated with relatively less low frequency energy. Loudspeakers could only produce such short duration signals if the signal is first modified in a complicated manner to correct for the speaker response in some direction.<sup>6,7</sup>

## CONCLUSIONS

Comparisons of the acoustical characteristics of a number of guns showed that a 0.38 calibre gun firing black powder blank cartridges is a suitable source of acoustical impulses. The gun was easily portable, and a repeatable, reasonably omni-directional source, radiating sufficient acoustical energy in all octave bands from 125 to 8000 Hz. It was further shown that not all guns were as satisfactory. In particular, the details of the wedge in front of the firing chamber influenced the directional properties of the gun. The smaller calibre guns tested did not provide adequate low frequency sound energy, and repeated a little less accurately.

Comparisons with spark and loudspeaker sources indicated that they were less satisfactory impulse sources. Spark sources tend to be lacking in low frequency sound energy, and involve bulky and potentially dangerous high voltage supplies. Spark sources appear to have somewhat similar directional properties and repeatability to the 0.38 calibre gun. Loudspeakers are more precisely repeatable, but again are bulky and hence much less portable. Loudspeakers usually have irregular frequency response characteristics that vary considerably with direction. It appears impossible to have a single loudspeaker that is satisfactorily omni-directional over a sufficiently broad frequency range.

Overall the 0.38 calibre gun was the most suitable source for measurements requiring acoustical impulses in rooms. Such a gun is a practical solution to the need to provide a single, omni-directional impulse from which decay times and early-to-late arriving sound ratios can be derived in octave bands from 125 to 8000 Hz.

## ACKNOWLEDGEMENTS

This paper is a contribution from the Division of Building Research, National Research Council of Canada, and is published with the approval of the Director of the Division.

## REFERENCES

1. "Airborne Isolation Measurements by Impulse Technique." J. Roland. Noise Control Engineering, Vol. 16, No. 1, p. 6-14 (1981).
2. "The Signal-to-Noise Ratio for Speech Intelligibility - An Auditorium Acoustics Design Index." H.G. Latham. Applied Acoustics, Vol. 12, No. 4, p. 253-320 (1979).
3. "A New Method to Acquire Impulse Responses in Concert Halls." A.J. Berkhout, D. deVries and M.M. Boone. J. Acoust. Soc. America, Vol. 68, No. 1, p. 179-183 (1980).
4. "An Efficient Algorithm for Measuring the Impulse Response Using Pseudorandom Noise." J. Borish and J.B. Angell. J. Audio Eng. Soc., Vol. 31, No. 7, p. 478-488 (1983).
5. "Impulse Testing Techniques for Auditoria." M. Barron. Applied Acoustics, Vol. 17, No. 3, p. 165-181 (1984).
6. "The Generation of Short Duration Acoustic Signals." J.C. Davies, J. McIntosh and K.A. Mulholland. J. Sound and Vibr., Vol. 76, No. 1, p. 77-82 (1981).
7. "Generation of Desired Signals from Acoustic Drivers." R. Ramakrishnan, M. Salikuddin and K.K. Ahuja. J. Sound and Vibr., Vol. 85, No. 2, p. 39-51 (1982).

# MEASUREMENT OF SOUND TRANSMISSION LOSS BY SOUND INTENSITY

A Preliminary Report

by

R.W. Guy and A. De Mey  
Centre for Building Studies  
Concordia University, Montreal

## ABSTRACT

The sound intensity technique is being implemented to measure sound transmission loss at the Centre for Building Studies acoustics test facility.

The use of the intensity technique for this purpose is being investigated in three main areas; validation with respect to standard techniques; determination of appropriate measuring procedure; exploiting the analytical capabilities of the technique. This paper presents some preliminary findings with respect to these areas.

## SOMMAIRE

Dans le laboratoire d'acoustique du Centre des études sur le bâtiment, la technique de mesure de l'intensité acoustique est introduite afin de déterminer la transmission du son.

A cet effet, l'utilisation de cette technique est examinée dans les trois domaines suivants: validation par rapport aux normes, détermination d'une procédure de mesure appropriée et exploitation des capacités analytiques de cette méthode. Cet article présente quelques conclusions préliminaires à cet égard.

## 1. INTRODUCTION

Traditionally the sound transmission loss of a panel or wall has been measured using the standard, classic approach as described by the ANSI/ASTM E90-81. However, the numerous contradictions between reported results based on this method [1] suggests the need for further investigation and this is being achieved through the application of the Sound Intensity Technique at the Centre for Building Studies at Concordia University, Montreal.

This new method has several advantages, for example: it gives the transmission loss directly without having to make corrections for the panel area and the absorption of the reception room; it eliminates the effect of flanking transmission; no restrictions are placed on the characteristics of the reception room, that is it neither has to be reverberant or anechoic; this fact eliminates the need of an actual transmission loss suite, although currently the existence of at least one reverberant chamber is exploited.

As opposed to pressure, intensity is a vector quantity and therefore provides directional information. In order to measure the transmitted intensity through a surface, only the component perpendicular to the surface is needed. However, to describe the power flow distribution, direction or transmission, three directional powerflow may be determined. The relative contributions to the total sound transmission of different sections of the test panel can be determined.

This paper presents the evaluation procedure employed to implement the Sound Intensity Technique. The technique was applied to the measurement of Sound Transmission loss through a panel with and without absorbent lined reveal; the results thus obtained were then compared with those obtained using the standard approach. In addition the effect of the lining was studied and the distribution of the intensity radiated through the panel determined.

## 2. METHODS TO MEASURE THE SOUND TRANSMISSION LOSS

The transmission loss is given by:

$$TL = 10 \log_{10} (\vec{I}_i / \vec{I}_t) \quad (1)$$

where  $\vec{I}_i$  is the incident intensity and  $\vec{I}_t$  the transmitted intensity.

### 2.1 Standard Approach

The standard method of measuring the Sound Transmission loss of a panel or wall involves the use of two vibration-isolated reverberation chambers that are separated partially or completely by the partition to be studied. The transmission loss is then:

$$TL = L_{ps} - L_{pr} + 10 \log_{10} (S/A) \quad (2)$$

where  $L_{ps}$  and  $L_{pr}$  are respectively the average sound pressure levels (dB) in the source and receiving rooms,  $S$  ( $m^2$ ) the partition's surface area and  $A$  ( $m^2$ ) the absorption of the receiving room.

It is assumed that the sound fields in both rooms are diffuse and that there is no flanking transmission.

## 2.2 Sound Intensity Approach

The determination of the transmission loss of a panel or wall is now done through the direct determination of both the intensity incident on and transmitted through the test partition.

The incident intensity  $I_i$  can be calculated from the measured space-averaged sound pressure  $P_{rms}$  in the source room assuming the sound field is diffuse [3].

$$|\vec{I}_i| = (P_{rms})^2 / 4\rho c \quad (3)$$

where  $\rho$  is the density of air and  $c$  the speed of sound in air. The accuracy of this equation has been verified by Crocker et al [3] by the direct measurement of the intensity through the aperture formed after removal of the test partition.

From equation (3) the following relationship between the incident intensity level  $L_{Ii}$  and the space averaged sound pressure level  $L_{pm}$  can be derived [4].

$$L_{Ii} = L_{pm} - 6 \quad (\text{dB}) \quad (4)$$

The transmitted intensity  $|\vec{I}_t|$  is measured on the receiving side of the panel as the intensity vector's component perpendicular to the panel's surface.

The sound transmission loss is then calculated from:

$$TL = L_{pm} - 6 - L_{It} \quad (\text{dB}) \quad (5)$$

where  $L_{It}$  is the transmitted intensity level.

### 3. TEST FACILITIES

#### 3.1 Transmission Loss Suite

The transmission loss suite of the Centre for Building Studies (C.B.S) at Concordia University consists of 2 rectangular rooms of differing dimensions. The larger room, the source room for all the reported experiments has a volume of approximately  $94\text{m}^3$ . The smaller room, the receiving room in this case has a volume of about  $32\text{m}^3$ . The test aperture between the rooms has an area of  $7.5\text{m}^2$  and the facility is shown in Fig. 1.

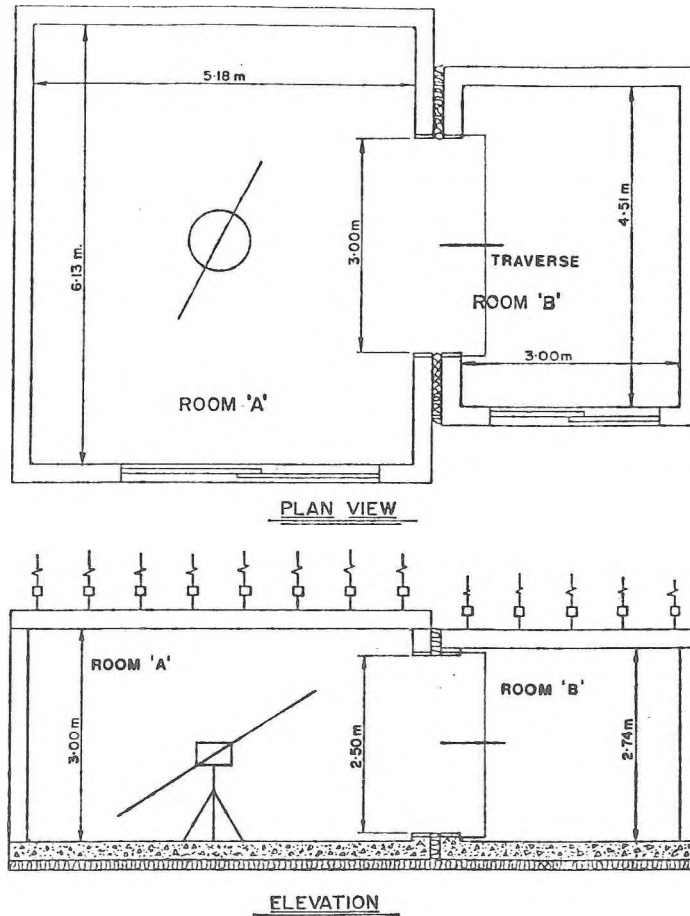


Fig. 1 General Layout of Transmission Loss Suite at the Centre for Building Studies, Concordia University.

The Schroder cut-off frequency is  $250\text{Hz}$  for the larger room and  $400\text{Hz}$  for the smaller one.

Diffusing elements consisting of one rotating and two stationary diffusers were located in the source room, and four stationary diffusers were located in the reception room.

The test facility is described in detail by Lang et al [6].

### 3.2 Test Wall

In order to accommodate the panel size tested, a heavy filler wall was constructed in the test aperture between the two rooms. The composition of the wall is given in Fig. 2.

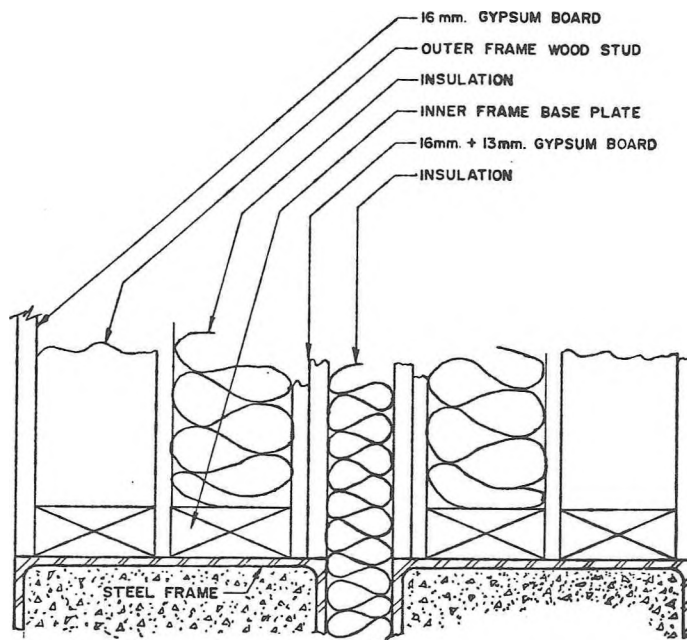


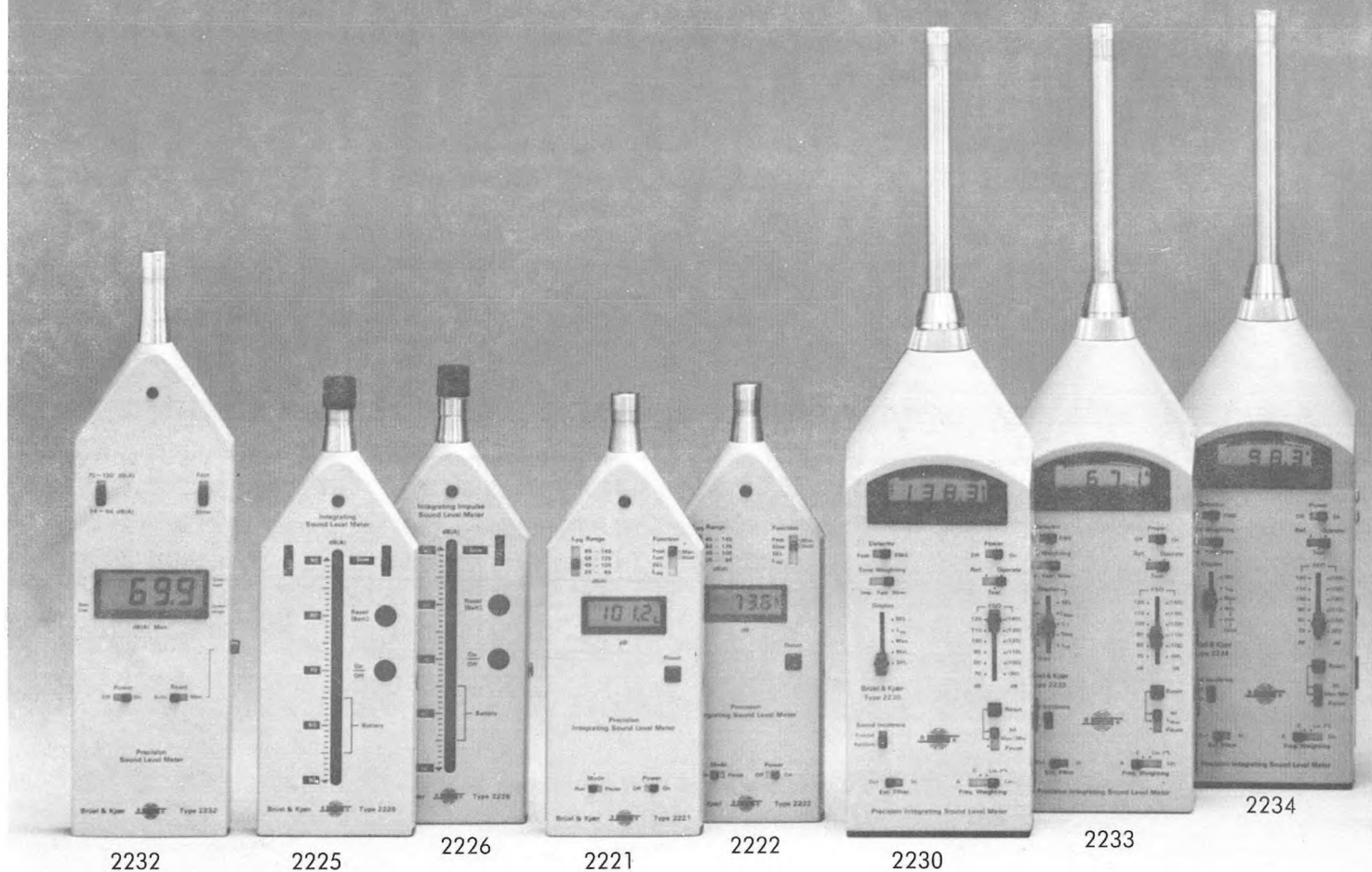
Fig. 2 Cross Section of Filler Wall at Base Plate

As can be seen the filler wall consists of two walls, mounted one in each room on their respective room's aperture and separated from each other by insulation material.

The STC value of the complete filler wall was 60.

The test panel was mounted flush to the source room, leaving a 39.4 cm. (15.5") deep reveal on the receiving side. The aperture was further splayed at 45° towards the reception room to minimize the effect of the remaining wall depth. The method of installation of the test panel is displayed in Fig. 3.

# WHAT'S ALL TH



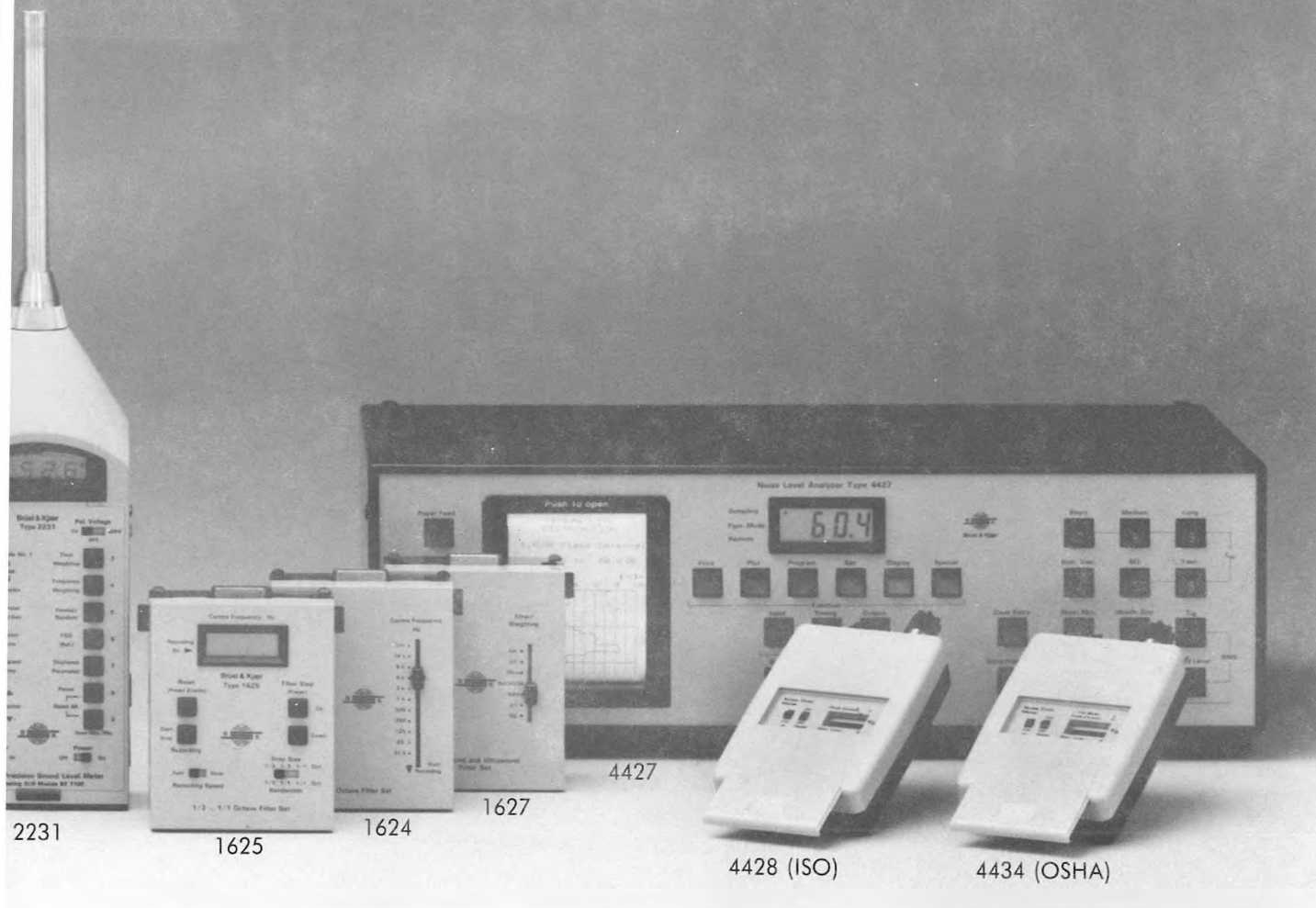
**Choose your instrument.** Whether it be the simple measurement of continuous noise or a highly complex record of industrial sound measurement, Bruel & Kjaer has the right combination of instruments for you.

The light weight, pocket sized precision sound level meter type 2232 gives an instant reading of the levels of continuous and pass-by noise. The equally-portable integrating sound level meter type 2225 will perform those functions as well as measuring impulsive, erratic and fluctuating noise. The type 2222 is a small Leq meter and the type 2230 is a precision Leq meter that can also adapt octave and  $\frac{1}{3}$  octave filter sets for frequency analysis. The type 2221 is our new "flagship" sound level meter. It is a digital instrument that can be programmed to perform almost any type of noise measurement.

Ideal for assessment of airport, traffic and community noise, the Noise Level Analyzer Type 4427 provides a statistical analysis of all noise activity on a continuous basis.

# NOISE ABOUT?

Bruel & Kjaer can tell you.



This entire family of Bruel & Kjaer instruments meets the highest international standards for accuracy and can handle your noise measurement problems for years to come. Put this family of B & K noise fighters to work for you.

 **BRÜEL & KJAER CANADA LTD.**

**MONTREAL:**  
Main Office  
90 Leacock Road,  
Pointe Claire, Quebec H9R 1H1  
Tel: (514) 695-8225  
Telex: 05821691 b + k pclr

**OTTAWA:**  
Merivale Bldg.,  
7 Slack Road, Unit 4,  
Ottawa, Ontario K2G 0B7  
Tel: (613) 225-7648

**TORONTO:**  
Suite 71 d,  
71 Bramales Road,  
Bramalea, Ontario L6T 2W9  
Tel: (416) 791-1642  
Telex: 06-97501

**LONDON:**  
23 Chalet Crescent,  
London, Ont.,  
N6K 3 C 5  
Tel: (519) 473-3561

**VANCOUVER:**  
5520 Minoru Boulevard, room 202,  
Richmond, BC V6X 2 A9  
Tel: (604) 278-4257  
Telex: 04-357517

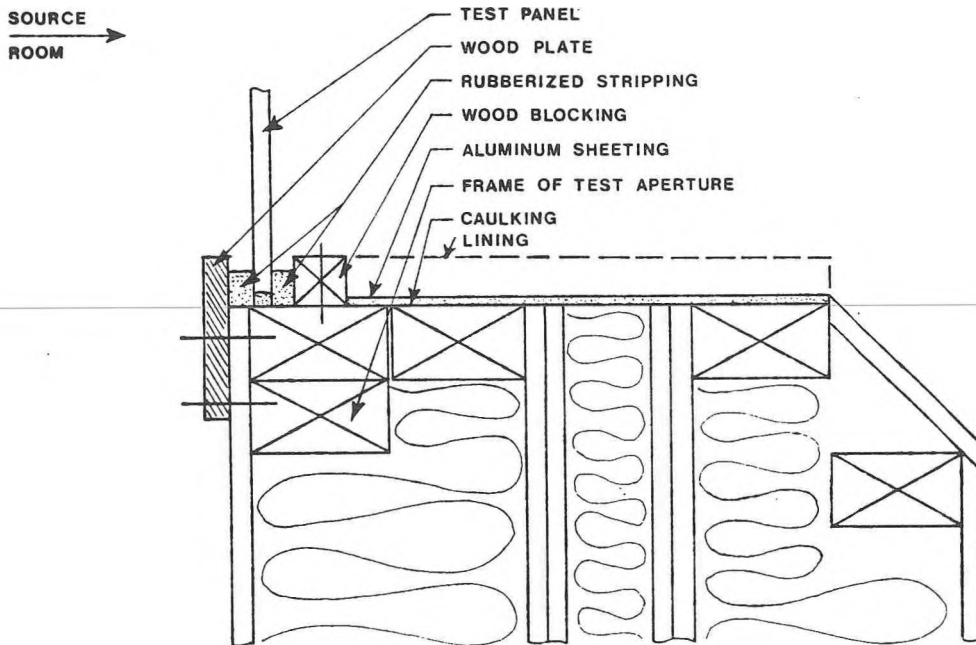


Fig.3 Mounting of Test Panel on Filler Wall

The test panel used was a 1.14 m x 1.14 m. (45" x 45") glass panel, 0.64 cm ( $\frac{1}{4}$ ") thick.

During the experiments reported here, the reveal on the receiving side was left either bare or lined with a 2.54 cm (1"), 5.08 cm (2") and 10.16 cm (4") absorbent material: Conaflex-F (by Blachford). For material properties, see Table 1.

TABLE 1. Absorption Coefficients of Conaflex F as Supplied by the Manufacturer.

Freq. (Hz)	Absorption Coefficient (%)*	
	F-100 (1")	F-200 (2")
125	9	28
250	19	68
500	57	90
1000	88	98
2000	96	98
4000	87	96

\*Test method ASTM C 423-66  
Test sample size 72 square feet

\*Approximate values derived from chart

\*Absorption coefficient for Conaflex F-400 (4") not available

## 4. TEST PROCEDURE

### 4.1 Standard TL Measurement

White noise was generated in the source room by two loudspeakers placed in the corners of the room opposite the test aperture.

The mean sound pressure levels in the source room were measured using a rotating microphone boom (B & K 3923). The microphone described a plane circular path at  $70^\circ$  from the horizontal and the length of the arm was 1.6 m, this configuration was chosen so that the microphone cleared the walls and stationary diffusers by at least 0.8 m (1/4 wave length at the 125 Hz centre frequency is 0.68 m). The minimum distance from the microphone to speakers was 1 m. and the period of a complete revolution of the microphone was 32 seconds.

In the receiving room, the mean sound pressure level measurement was performed in the same manner as in the source room, however because of its smaller size, the length of the arm was changed to .95 m and the turntable was tilted at  $60^\circ$  from the horizontal.

The reverberation time in the receiving room was calculated from the averaged decay points (16 per second and 50 decay samples) with the turntable in the same position as described above and with the microphone rotating. A linear regression analysis was used in the range -5 dB below the upper decay points down to 10 dB above background level.

All measurements were computer controlled and fed to a third octave analyser. In this case, the Sound Intensity Analyser type 2134/3360 from Bruel and Kjaer.

### 4.2 Sound Intensity Method

The incident intensity was calculated from the mean sound pressure level as measured by the reverberant room method described earlier.

The transmitted sound intensity was measured directly using the B & K Sound Intensity Microphone Probe type 3519, using the face-to-face microphone configuration. The  $\frac{1}{2}$ " microphones with 12 mm spacer were chosen which gives a useful frequency range, of 125 Hz to 5 k Hz with an accuracy of  $\pm 1$  dB assuming a monopole source

The intensity radiated through the panel was measured at 5.08 cm. (2") behind the surface employing an array of 81 evenly distributed points over the surface; this choice of measuring parameters will be discussed later. It became obvious during the preliminary test phase that in the presence of the reveal, the transmitted sound intensity used in the determination of the transmission loss had to be measured on the receiving room side of the reveal where it merges into the filler wall's surface. The same array of points was used.

During the measurements the microphone probe was mounted on a mechanical traverse system that enabled the microphones to be fixed during each measurement interval. It was then moved by hand from point to point, although later developments will include the automation of this traverse.

All data was stored on disk through the use of the Remote Indicating Unit ZH 0250 (B & K).

In order to avoid reverberant field effects on the intensity method measurement accuracy the three non-parallel walls of the receiving room were covered with a thick absorbent material: Conaflex F-400. Naturally this material was removed for the corresponding sound pressure measurements.

#### 4.2.1 Estimation of the Phase Errors in the Intensity Measurements

Given the experimental conditions described above, the reactivity of the sound field was determined in both measurement planes for the purpose of estimating the errors resulting from the phase mismatch between the two measuring channels. The reactivity is the ratio between the sound pressure and the sound intensity.

The error  $L_{er}$ , defined as the difference between the measured intensity level (dB) and the true intensity level (dB) can be calculated from [8]:

$$L_{er} = -10 \log_{10} \left( 1 - \frac{I_{re} \cdot P_t^2}{P_{rc}^2 \cdot I_{me}} \right) \quad (\text{dB}) \quad (6)$$

where  $P_{re}$  (Pa) is the sound pressure in a completely reactive field,  $I_{re}$  ( $\text{W}/\text{m}^2$ ) the apparent, residual intensity associated with it, and  $P_t$  (Pa) and  $I_{me}$  ( $\text{W}/\text{m}^2$ ) respectively, the actual measured sound pressure and intensity.

The measurement errors as given by (6) were relatively high (up to 3 dB) at the extreme lower end of the frequency range. However, for frequencies equal to or higher than 250 Hz, they were found to be less than 1 dB at 5.08 cm (2") from the test panel and less than .5 dB at the receiving room side of the reveal.

If the receiving room had not been lined, the reactivity of the sound would have been higher, thus increasing the measurement errors even further.

### 5. PRELIMINARY TESTS

Although the use of the sound intensity technique for transmission loss measurement has been established by others, experimental details of the procedure are still vague and left up to the user. For example, typically what relationship exists between measuring point distance and included radiation surface area. The solutions available are quite variable

Cops [5], for example uses a mesh size of 19.5 cm x 20.75 cm with a measurement distance of 4 cm, while Fahy [4] uses the same distance but for a mesh of 4.5 cm x 7.5 cm. Therefore, before the actual transmission loss tests it was necessary to determine these parameters experimentally. During these measurements only the transmitted intensity level was determined, the incident power being held constant for each of the series.

### 5.1 Influence of Absorbent Material in the Reception Room

Intensity measurements were made with and without absorbent material in the reception room. In the former case, three non-parallel walls of the reception room were covered with Conaflex F-400.

As expected the values of the measured transmitted intensity levels for the unlined case were lower than those obtained in the presence of the absorbent material although the differences were very small with a maximum discrepancy of 1 db.

However, in order to avoid any effect of the reverberant field on the measurement accuracy involving sound intensity measurements the reception room was always lined as described.

### 5.2 Averaging Time

The averaging time is an important parameter in a measurement procedure both for accuracy and for total duration of test. The object was to minimize time without loss of accuracy.

For an array of 81 points the transmitted intensity was measured using different linear averaging times: 4,8,16 and 32 sec. The results obtained were compared with the 32 sec. averaging time which was deemed accurate for steady state measurement.

The intensities averaged over the total test panels surface were very similar in all cases ( $\pm .5$  dB). However, after a comparison of the results point for point, a linear averaging time of 8 sec. was chosen since the maximum point deviation from the 32 sec. measurement did not exceed 1dB.

### 5.3 Mesh Size

Four different mesh sizes were tested 38.1 cm x 38.1 cm (15" x 15"), 22.86 x 22.86 cm (9" x 9"), 16.33 x 16.33 cm (6.5" x 6.5"), 12.7 x 12.7 cm (5" x 5") giving a total number of measuring points of respectively 3 x 3 (9), 5 x 5 (25), 7 x 7 (49), 9 x 9 (81) evenly distributed over the test panel's surface. No attempt to increase the total number of points has been made because of the time penalty incurred. Each time the power flow was measured at the centre of the subarea so created at a distance, (test panel to centre of microphone pair) of half the mesh size.

The results with respect to the average transmitted intensity show the following (Fig. 4):

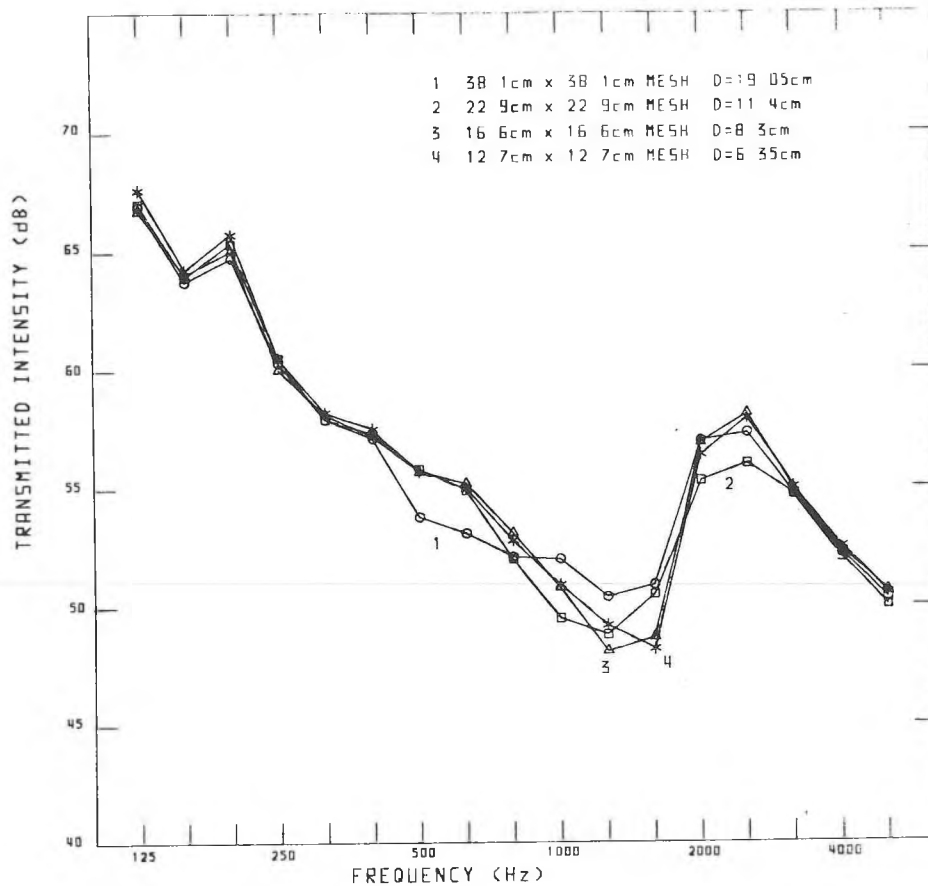


Fig 4 The Influence of the Mesh Size on the Measured Transmitted Intensity ( $t_{av} = 8$  sec)

Little difference is seen between the results of the 7 x 7 and 9 x 9 meshes, also with one exception differences were less than .5 dB.

For the 5 x 5 mesh, the only large deviation observed was around the coincidence frequency in the 2500  $H_z$  third octave band. The peak in the transmitted intensity, which gives rise to the coincidence dip in a transmission loss plot, is seen to be much lower and wider.

The results of the 3 x 3 mesh were more irregular together with large differences from the smaller mesh sizes.

For the present purpose, the smallest mesh size was chosen to avoid inaccuracies and because of the more detailed information possible with respect to establishing the contours of radiated intensity distribution.

#### 5.4 Measurement Distance

In order to optimize the measurement distance the transmitted intensity was measured at several distances from the test panel.

With regard to the 9 x 9 mesh the distances chosen were 3.81 cm (1.5"), 5.08 cm (2"), 7.62 cm (3"), 10.16 cm (4") and 12.7 (5").

Certain trends in the results can be observed (Fig. 5).

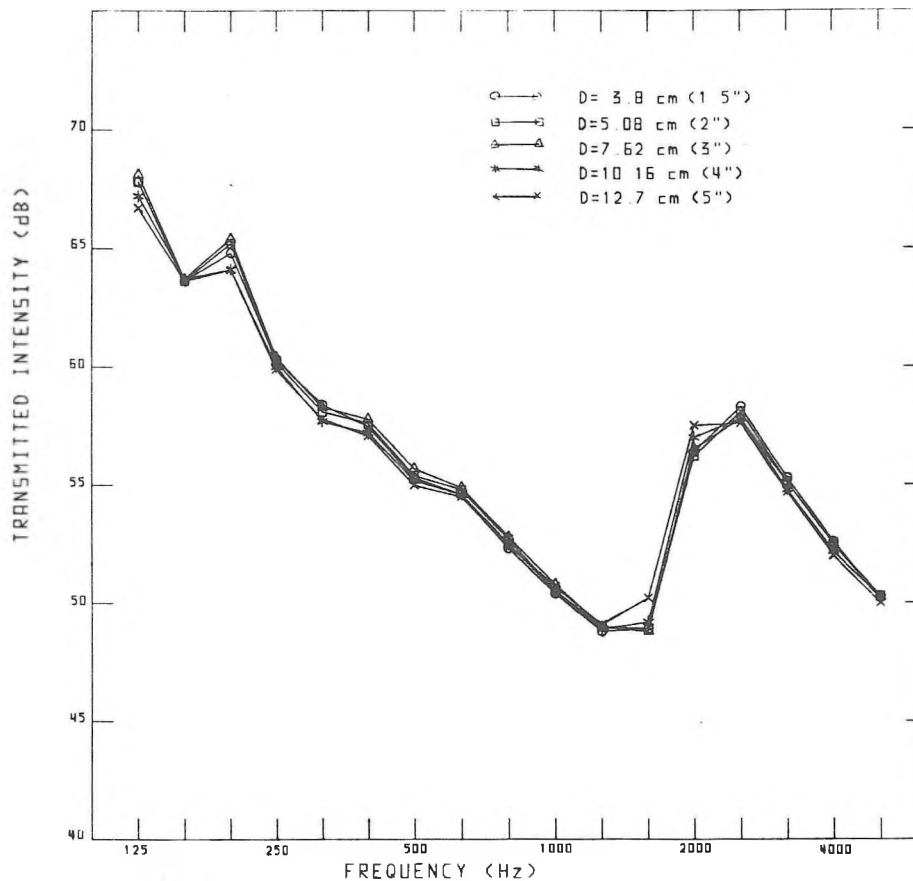


Fig. 5 Influence of Measurement Distance  
 12.7 cm x 12.7 cm Mesh  $t_{av} = 8$  sec

When the distance is smaller than 10 cm (4"), there is very little difference (+ .6 dB) between results. However,  $L_t$  increases with increasing distance below coincidence. This trend reverses above coincidence.

The larger the measurement distance the less prominent the coincidence peak, with the measured coincidence frequency finally falling to the next lower third octave frequency band.

As a consequence the measurement distance chosen was 5.08 cm (2").

## 6. TRANSMISSION LOSS TESTS

### 6.1 Comparison of Standard and Intensity-Based Transmission Loss Measurement

For the sake of comparison between the two measurement methods and in order to take account of the reveal effect, the transmitted intensity reported in this section was measured on the reception room side of the reveal.

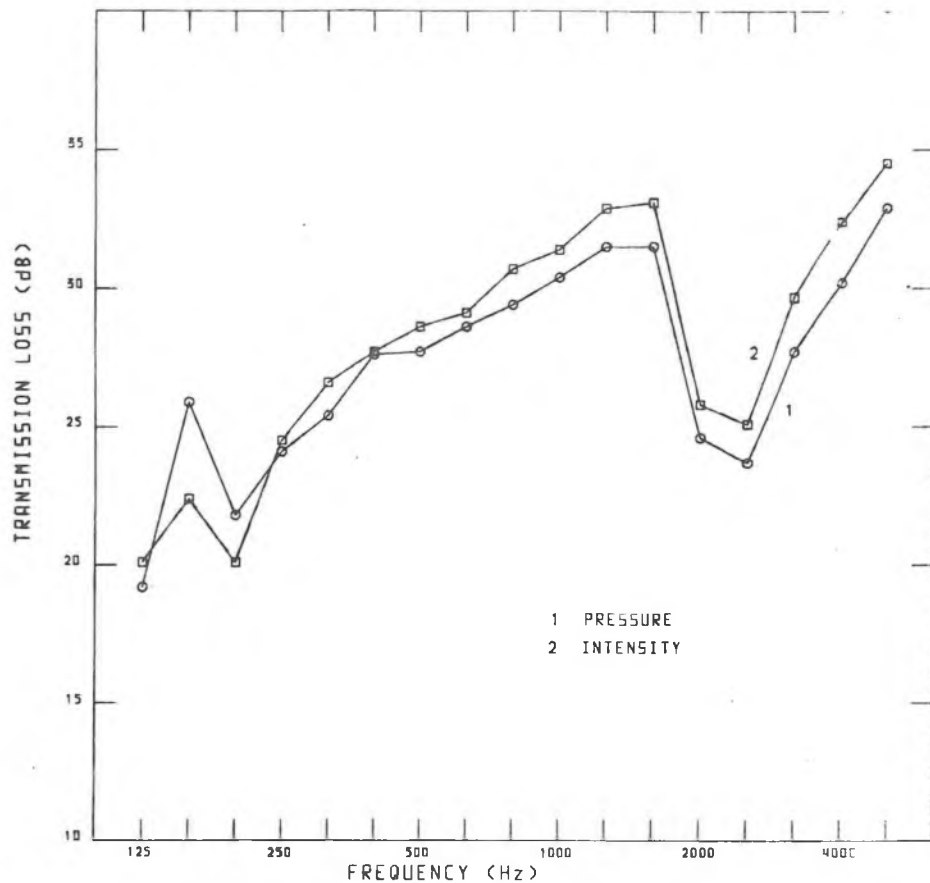


Fig. 6 Comparison between Standard and Intensity-Based  
Transmission Loss Measurement  
12.7cm x 12.7cm Mesh  $t_{av} = 8 \text{ sec}$

As shown in Fig. 6 for the reveal left bare the results obtained are generally very similar with a maximum difference of 2 dB. Greater differences can be seen at lower frequencies and this is probably due to the small reception room size. The same trends were observed with the reveal lined.

Overall, one may conclude that the earlier reported technique validity, Crocker et al [3], Fahy [4], and Cops [5], has been demonstrated.

## 6.2 Lining of the Reveal

The transmitted intensity was again measured on the reception room side of the reveal.

Fig. 7 shows that the effect of lining thickness increases gradually over most of the frequency range, peaking in effect between, 1KH and 2KH<sub>z</sub>.

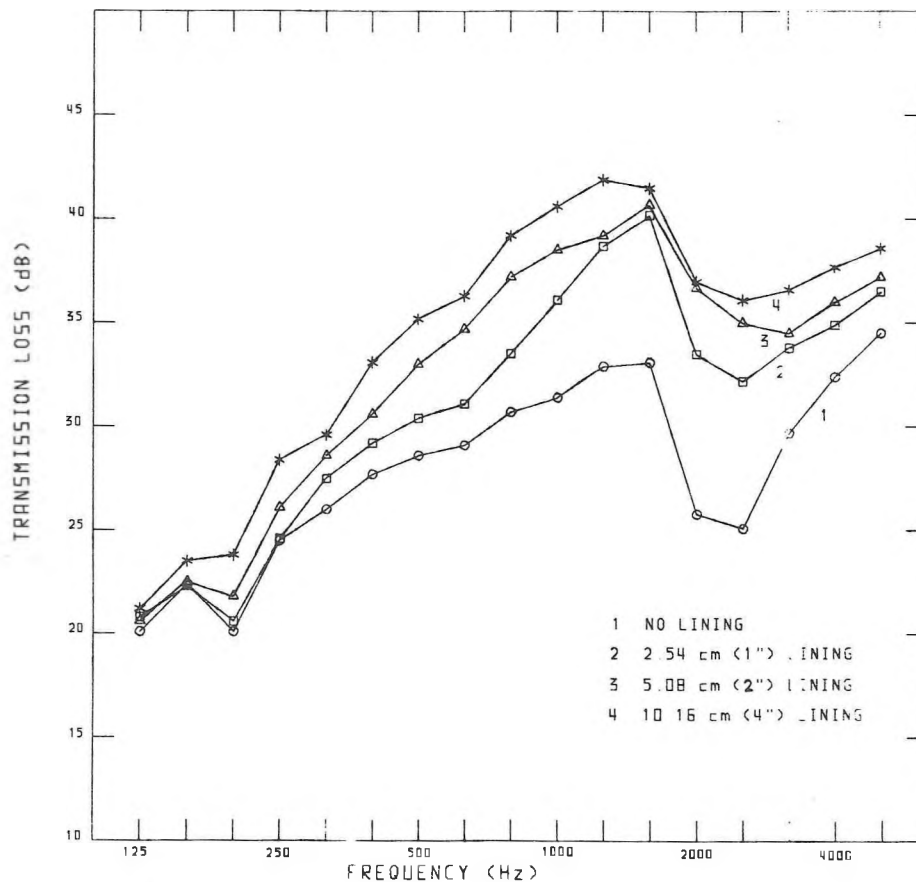


Fig. 7 Influence of Lining the Reveal on the Total Transmission Loss  
 12.7cm x 12.7cm Mesh  $t_{av} = 8$  sec

Generally the thicker the lining, the higher the measured transmission loss, but only as a function of lining material absorption coefficient as one might expect (see Table 1).

Little effect is observed at the lower frequencies and this is probably due to the low frequency absorption characteristics of the lining material, although the prominence of grazing mode transmission with respect to the lining at low frequencies might also influence this result.

When the transmitted intensity is measured directly behind the test panel at a 5 cm (2") distance, the measured transmission loss in the cases when the reveal was lined with 0, 2.54 cm (1") or 5.08 cm (2") were the same, as can be seen in Fig. 8.

Therefore, the transmission loss of the test panel alone is not influenced by the lining, and this suggests that the panel vibration is only loosely coupled to the airborne modes of energy transfer.

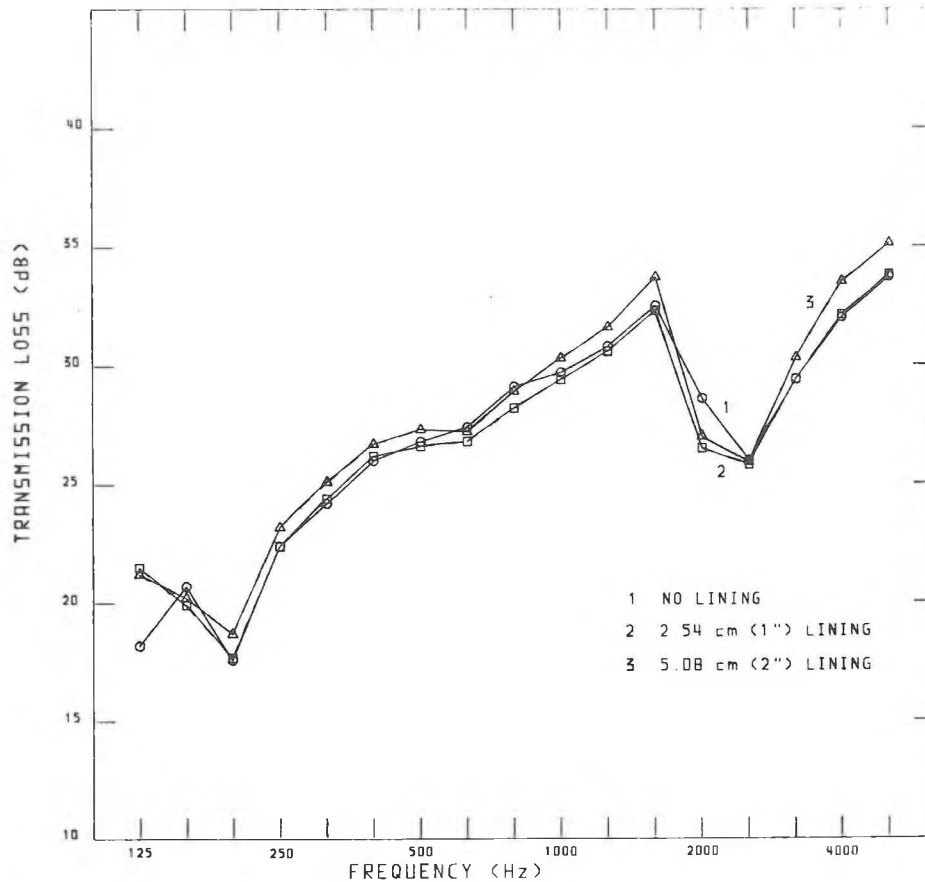


Fig. 8 Influence of Lining the Reveal on the Transmission Loss Measured at the Panel  
 12.7cm x 12.7cm Mesh D= 5.08cm (2")  $t_{av} = 8$  sec

### 6.3 Distribution of the Intensity Radiated Through the Test Panel

This topic has been studied theoretically by for example Maidanek [7] and recently also experimentally by Fahy [4] using the sound intensity technique. For frequencies below coincidence the theoretical model demonstrates that the wave pattern at the edges of a finite plate cause most radiation, in contrast with an infinite plate. It is further suggested that for these frequencies only a strip of plate around the edges radiate sound power. Above the coincidence frequency, panels radiate from their whole surface, although the experimental results of Fahy did not completely agree with this.

The basic experiment has been repeated; the radiated intensity was for this purpose measured directly behind the test panel at a distance of 5.08 cm (2") and contours of equal normal intensity were then plotted; results are shown at 250 Hz (Fig. 9), and 5000 Hz (Fig. 10).

At very low frequencies (Fig. 9) the panel is radiating predominantly through the corners. The intensity transmitted through a small center portion of the panel is much lower and therefore negligible.

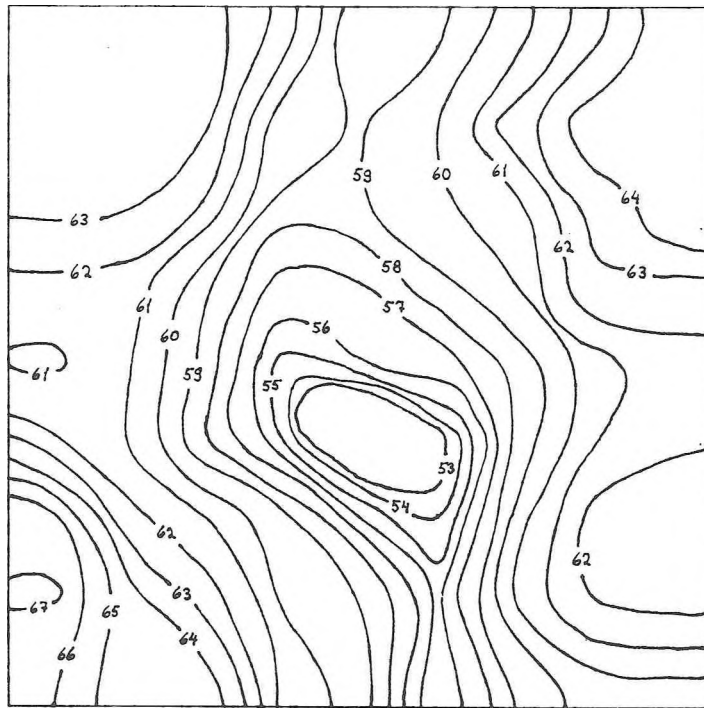


Fig.9 Intensity Contours Normal to the Panel Surface at 250 Hz

At mid frequencies closer to the coincidence frequency it was found that the center portion contribution becomes larger, however greater intensity is found around the panel border and the gradients are found to be much steeper at the edges than at lower frequency. Closer to and at the coincidence frequency the strong intensity around the border of the plate remains, but the center portion of the panel tends to radiate much more than at lower frequencies.

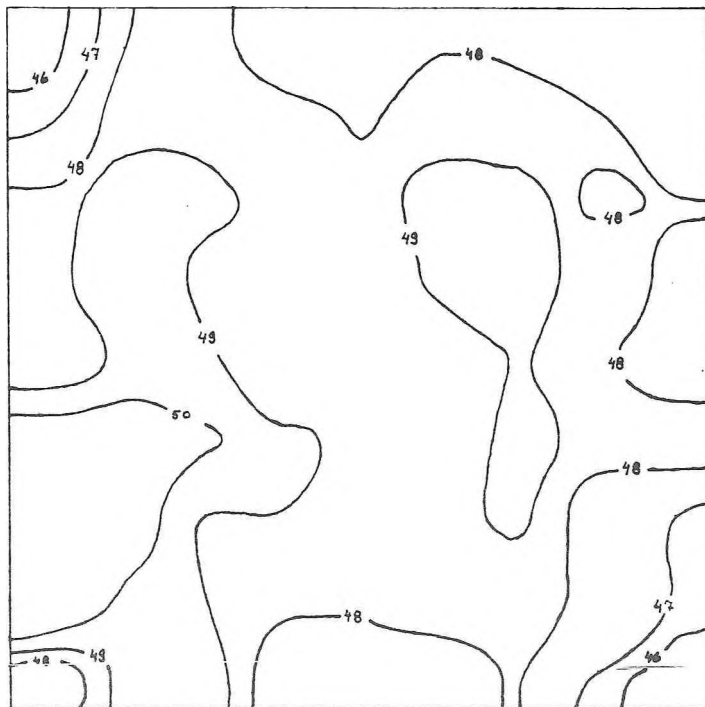


Fig.10 Intensity Contours Normal to the Panel Surface at 5000 Hz

Above the coincidence frequency (Figure 10) a quite uniform radiation over the whole surface of the panel can be observed.

#### 6.4 Fault Finding

The capabilities of the sound intensity technique with regard to the detection of construction or material deficiencies was also examined.

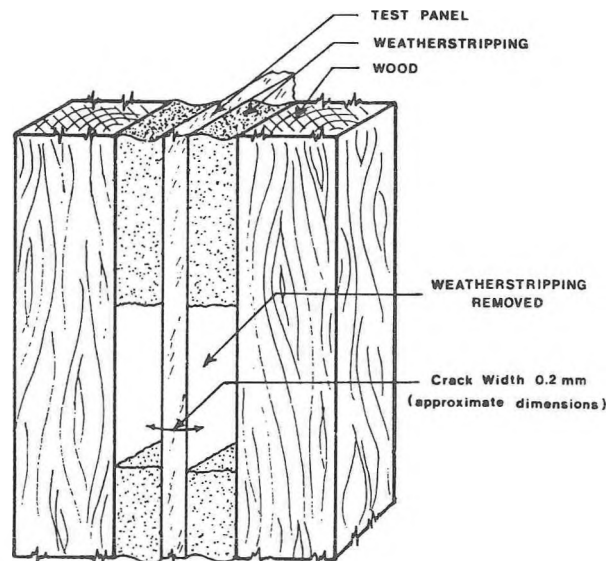


Fig. 11 Scheme of Fault Introduced by Removing Weatherstripping.  
Strip Length 9.5 cm; Crack Width 0.2 mm (approximate dimensions)

For this purpose a fault was introduced by removal of the weatherstripping on both sides of the panel as shown in Fig. 11. The exposed portion revealed a crack approximately 9.5 cm long and 0.2 mm wide between the panel edge and its mounting frame.

Intensity measurements were made directly behind the test panel at a distance of 5.08 cm (2"). The intensity pattern obtained was investigated for observable irregularities. It was found that close to the fault, the values of transmitted intensities were generally higher than at the same points before the fault was introduced. The differences in local intensity were slight at lower frequencies, up to 3dB at 250 Hz, increasing to 10 dB at 2000 Hz and falling lower again beyond this frequency.

As can be seen in Fig. 12 the effect is indicated by the intensity contours. However, when comparing the overall sound transmission loss before and after the introduction of the fault (see Figure 13) the influence of the fault is only noticeable above 800 Hz and leads to a maximum difference in overall transmission loss of 2.5 dB at 1KHz with smaller, to negligible differences over the rest of the frequency range.

Such a fault could easily be overlooked by consideration of the overall spectrum alone.

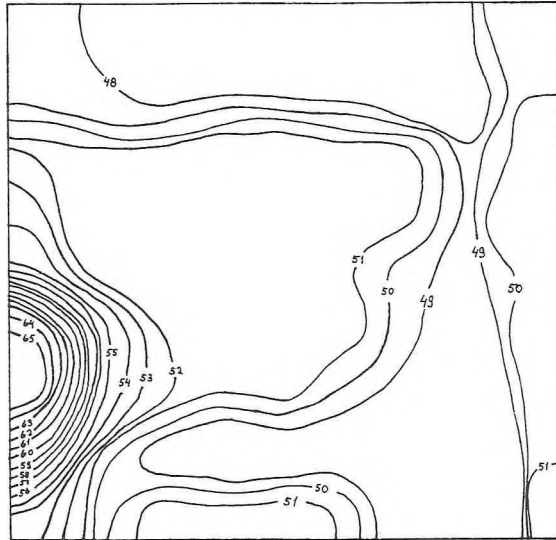


Fig. 12 Fault Finding. Influence of Removing Weatherstripping at 1600 Hz

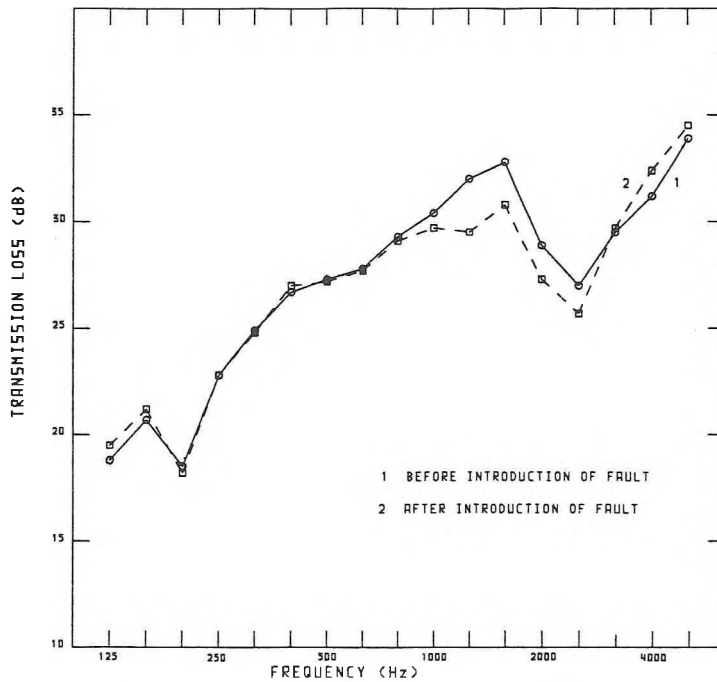


Fig. 13 Comparison between the Transmission Loss of the Test Panel before and after the Introduction of the Fault

12.7cm x 12.7cm Mesh  $t_{av} = 8$  sec  $D = 5.08$ cm (2")

## CONCLUSION

The validation of the intensity-based transmission loss measurement has been confirmed. A detailed measurement procedure has been established, and the analytical capabilities of the new method exploited to determine the influence of lining the reveal of the test panel with absorbent material. The overall transmission loss has been shown to increase with increasing thickness of absorbent lining. However the intensity measurement technique indicates that the panel radiation is not influenced by the presence of the lining, such a conclusion would not have been possible employing the standard reverberation room technique.

It was also demonstrated that the intensity technique can be used to identify the existence of untoward sound transmission paths as part of a normal measurement procedure.

## ACKNOWLEDGEMENT

This work was supported from individual operating grant A0374 of the National Science and Engineering Research Council.

## REFERENCES

- [1] R.W. Guy, A. De Mey, P. Sauer, "The Effect of Some Physical Parameters Upon the Laboratory Measurement of Sound Transmission Loss", C.B.S. Report No. 105., October 1983.
- [2] ANSI/ASTM E90-75, "Laboratory Measurement of Airborne Sound Transmission Loss of Building Partitions".
- [3] M.J. Crocker, P.K. Raju, B. Forssen, "Measurement of Transmission Loss of Panels by the Direct Determination of Transmitted Acoustic Intensity", Noise Control Engineering, Vol. 17, July - August 1981, p. 6-11.
- [4] F.J. Fahy, "Sound Intensity Measurement of Transmission Loss", Proceedings of the Institute of Acoustics, 1982, P. B5.1 - B5.4.
- [5] A. Cops, "Acoustic Intensity Measurements and their Application to the Sound Transmission Loss of Panels and Walls", Internoise 83, P. 567-570.
- [6] M.A. Lang, J.M. Rennie, "Qualification of a 94 Cubic Meter Reverberation Room Under ANS S1.21", Noise Control Engineering / September - October 1981, P. 64-70.
- [7] R.H. Lyon, G. Maidanik, "Response of Ribbed Panels to a Reverberant Acoustic Field", J.A.S.A., 1962, Vol. 34, P. 623.
- [8] Per Rasmussen, "Phase Errors in Intensity Measurements", B & K Application Note, May 1984.

# AN ACOUSTICAL EXPLORATION TECHNIQUE FOR DETECTING OIL TRAPPED UNDER SEA ICE

H.W. Kwan and H.W. Jones  
Technical University of Nova Scotia  
P.O. Box 1000  
Halifax, Nova Scotia B3J 2X4

## ABSTRACT

This paper reviews in outline the theoretical and practical aspects of an acoustical method of detecting oil trapped under sea ice. Following discussion of the theoretical problems, information relating to acoustical mode conversion in the ultrasound reflected from the lower side of the ice is presented. An experiment in a large salt water tank, with about 80 cm of ice, is described and the results are related to theory which is presented. A commentary on the lessons learned from this experiment is given. An outline of the design for a prototype field apparatus is presented.

## SOMMAIRE

On présente un bref aperçu des aspects pratique et théorique d'une méthode acoustique pour détecter l'huile emprisonnée sous les glaces océaniques. On discute entre autre des modes de propagation acoustique de l'onde ultrasonique réfléchié du dessous de la glace. Des mesures effectuées dans un réservoir d'eau salée avec 80 cm de glace sont comparées avec la théorie et les conséquences de cette expérience discutées. Finalement les grandes lignes d'un appareil prototype sont présentées.

## INTRODUCTION

In earlier papers (1,2,3) introductory considerations relating to an acoustical method of detecting oil under ice were presented. These considerations included a study of the physical properties of sea ice and oil, and a summary of acoustical methods which had been attempted (unsuccessfully) on earlier occasions. A new method of using ultrasound was explored in outline. The principle of this method is shown in Figure 1. A short pulse of ultrasound is transmitted into the ice, this pulse is reflected and mode converted at the interface between the ice and the oil or water. The two returning pulses, one, a compressional wave and the other a shear wave, are received and recorded. The received signals carry two pieces of information, i.e., that relating to the thickness of the ice, and that which indicates the presence of oil or water in contact with the ice. The incident wave can be either compressional or shear; we have argued on earlier occasions that compressional waves appear to be a better choice for practical and theoretical reasons (3). The relative amplitudes of the returning waves indicate the presence, or otherwise, of oil. The thickness of oil which can be detected appears to be quite small. It is estimated that this thickness can be less than half the sound wavelength, and it may be possible to detect oil layers of 0.5 cm or less in practical circumstances.

Many practical problems exist in the design of a piece of apparatus for economical and regular use in the field. We base the following commentary on the limited amount of field experience which has been obtained to date. In field experiments oil was detected under 80 cm of salt water ice; the oil thickness varied from about 2 cm to less than 1 cm. There are difficulties due to unwanted artifacts in experimental data. It becomes important to recognize such artifacts and reduce their influence in data interpretation, particularly if automatic data assessment is used.

## Interfacial Effects

The method we are describing depends on the interfacial effects at the bottom of the ice. It is necessary to be able to evaluate the results to be expected, consequently the required theory is outlined in the following paragraphs.

The reflection and refraction of compressional or shear waves at an interface between two materials is a complicated phenomenon. When a wave is incident on an interface, reflection, transmission and mode conversion can occur. The special circumstances of this case relating to transmission from solid to liquid and solid to visco-elastic liquid have been studied in general terms (4,5,6,7). If we suppose a general case in which we are dealing with transmission from visco-elastic to visco-elastic media, then limiting conditions allow us to evaluate all the cases of practical interest in these circumstances.

Figure 2 shows the geometry relating to the boundary and the sound waves incident upon it. The reflection and refraction coefficients are determined by solution of a set of linear equations which arise from the need to conserve displacement and force at the boundary. The coefficients are obtained from:

$$A_{\ell} R_{\ell} = B_{\ell} \quad (1)$$

where  $\ell = 1, 2$  for incident compressional or shear waves, respectively and

where,

$$A_1 = \begin{pmatrix} \sin \zeta_{111} & \cos \zeta_{112} & -\sin \zeta_{121} & \cos \zeta_{122} \\ \cos \zeta_{111} & -\sin \zeta_{112} & \cos \zeta_{121} & \sin \zeta_{122} \\ -\rho_1 S_{11} \cos 2\zeta_{112} & \rho_1 S_{12} \sin 2\zeta_{112} & \rho_2 S_{21} \cos 2\zeta_{122} & \rho_2 S_{22} \sin 2\zeta_{122} \\ (\rho_1 S_{12}^2 / S_{11}) \sin 2\zeta_{111} & \rho_1 S_{12} \cos 2\zeta_{112} & (\rho_2 S_{22}^2 / S_{21}) \sin 2\zeta_{121} & -\rho_2 S_{22} \cos 2\zeta_{122} \end{pmatrix}$$

$$B_1 = \begin{pmatrix} -\sin \theta_1 \\ \cos \theta_1 \\ \rho_1 S_{11} \cos 2\zeta_{112} \\ (\rho_1 S_{12}^2 / S_{11}) \sin 2\theta_1 \end{pmatrix}, \quad B_2 = \begin{pmatrix} \cos \theta_2 \\ \sin \theta_2 \\ -\rho_1 S_{12} \sin 2\theta_2 \\ -\rho_1 S_{12} \cos 2\theta_2 \end{pmatrix}, \quad R_1 = \begin{pmatrix} R_{111} \\ R_{112} \\ R_{121} \\ R_{122} \end{pmatrix}$$

and  $R_{\ell mn}$ , are the displacement reflection and refraction coefficients. The suffix  $m$  refers to the medium through which the wave is passing and suffix  $n$  refers to compressional or shear waves when its value is 1 or 2 respectively. The angle  $\theta_{\ell}$  is the angle between the incident wave and the  $Y$  axis. The various angles  $\zeta_{\ell mn}$  (which are the complex angles) are related through their sines to the velocity of propagation ratios as the complex Snell's law:

$$\sin \zeta_{\ell mn} = S_{mn} \sin \theta_{\ell} / S_{1\ell}, \quad \text{for } \ell, m, n = 1, 2 \quad (2)$$

where  $S_{m1}^2 = (\lambda_m + 2\mu_m) / \rho_m$ ,  $S_{m2}^2 = \mu_m / \rho_m$

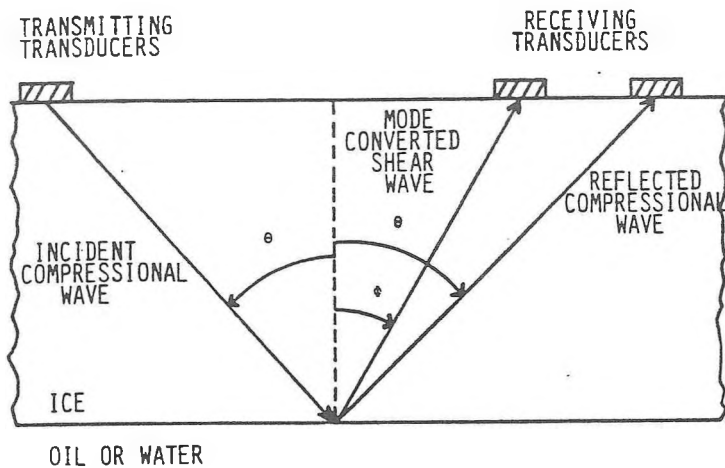


Figure 1  
Schematic of Experimental set up.

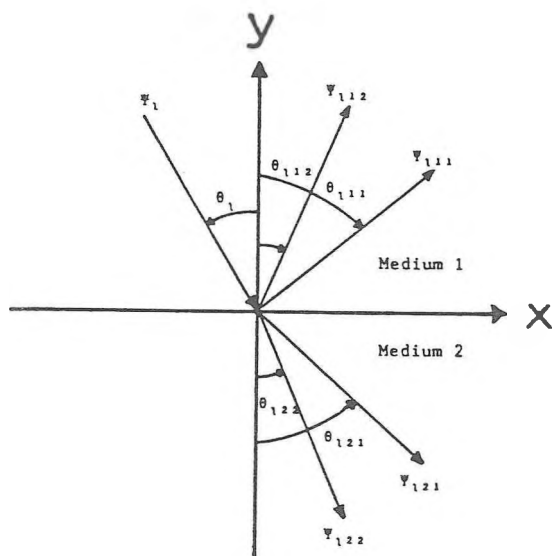


Figure 2  
Reflection and Refraction Phenomena at the interface  $Y = 0$ .

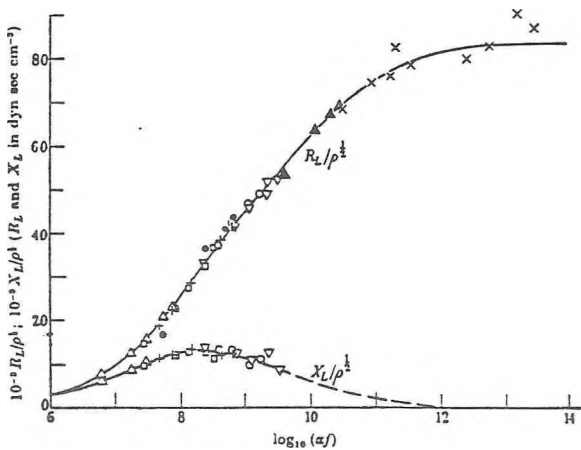


Figure 3  
Resistive and reactive components of a high viscosity oil, for various temperatures, as a function of frequency, ( $\alpha = \eta_T/\eta_{300}$ .  $\eta$  is viscosity at indicated temperature. After Barlow and Lamb, 1959)

$\lambda_m$  and  $\mu_m$  are the complex Lamé's elastic constants of material, and  $\rho_m$  is the density of material. It is to be noted that the matrices associated with equation (1) have been corrected to remove errors contained in the original publication.

The complex properties of visco-elastic substances are dependent on several factors, among them the temperature and frequency of the ultrasound. Figure 3 shows typical data for various oils. As a consequence of these factors, the solutions of equation (1) will also depend on the conditions which are related to a particular experimental problem.

Curves 1 and 2 in figure 7 are an estimate of the limits of the relative ratio of the compressional to shear waves returned from the lower surface for an oil in contact with the ice by comparison to water next to the ice. Curve 1 is the high frequency limit; curve 2 is the low frequency limit obtained from the use of equations (1) and (2). In practice, experimental results can be expected to lie between these boundaries.

### Experimental Work

The experiments on salt water ice at lower frequencies require a large sheet of thick ice and Esso Resources Canada Ltd allows us to use their large outdoor brine tank at Calgary. Figure 4a and b show part of the ice sheet on the tank and a block of ice taken from the site of our experiments. The ice on the tank was about 80 cm thick and made from brine, frozen from the top surface by winter temperatures assisted by refrigeration pipes laid on the surface. There was a relatively large volume of unfrozen water in the tank; probably less than 20% of the original brine was frozen. Consequently, the ice is a fair approximation to the sea ice, except that its lower surface is flat (see Figure 4b) because of the lack of wave action and ridging during freezing.

The transducers which were used operated at a basic frequency of 144 kHz. The transducers were driven by a large amplitude tone-burst provided by a broadband power amplifier. The receiving transducer was similar to the transmitter. The received signals were transmitted via a head amplifier and a coaxial line to a variable bandwidth filter and other receiving electronics. Figure 5 shows a typical trace of a received signal. Measurements were made for angle  $\theta$  (see Figure 1) in the range of  $5^\circ$  to  $30^\circ$ , with water in contact with the ice. Next a depression 2.5 cm deep was melted in the underside of the ice, using the method illustrated in Figures 6. This depression was filled with oil, and a set of measurements with oil in contact with the ice was made. Two points should be stressed; first the dimensions of the melted area containing the oil were sufficiently large to "contain" the main lobe of incident beam of the transmitting transducer. This means that the received signal came primarily from the oil-filled region. The second point concerns the displacement of the water by the oil from the ice surface. Much thought was given to this point and a variety of methods for placing the oil were discussed. Finally the oil was just released from a can into the cavity. Immediately after oil was in place, repeated readings were obtained. During the course of these readings, the oscilloscope traces changed, showing that the water was displaced from the surface as the oil insinuated itself into the cracks of the ice. Later borings showed that the oil had penetrated about 30 cm into the ice over a period of 24 hours. An estimate of the oil transport suggests that about



Figure 4(a)  
General view of Basin.



Figure 4(b)  
A block of ice from the Basin.

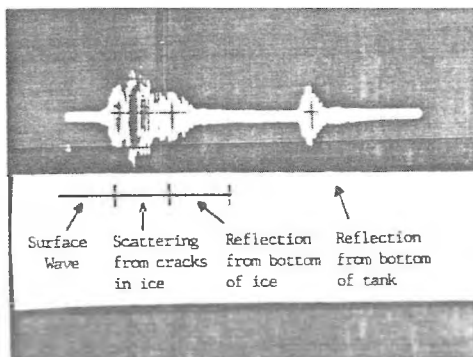


Figure 5  
Typical trace of a signal.  
Vertical = 50 mV/div.  
Horizontal = 0.2 msec/div.

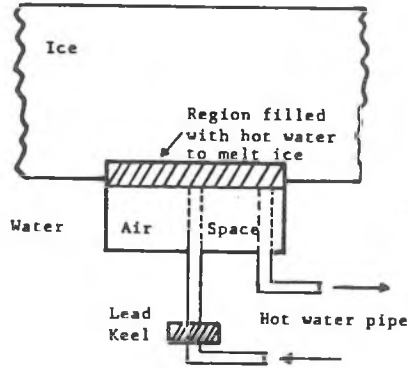


Figure 6  
Experimental arrangement for melting ice.

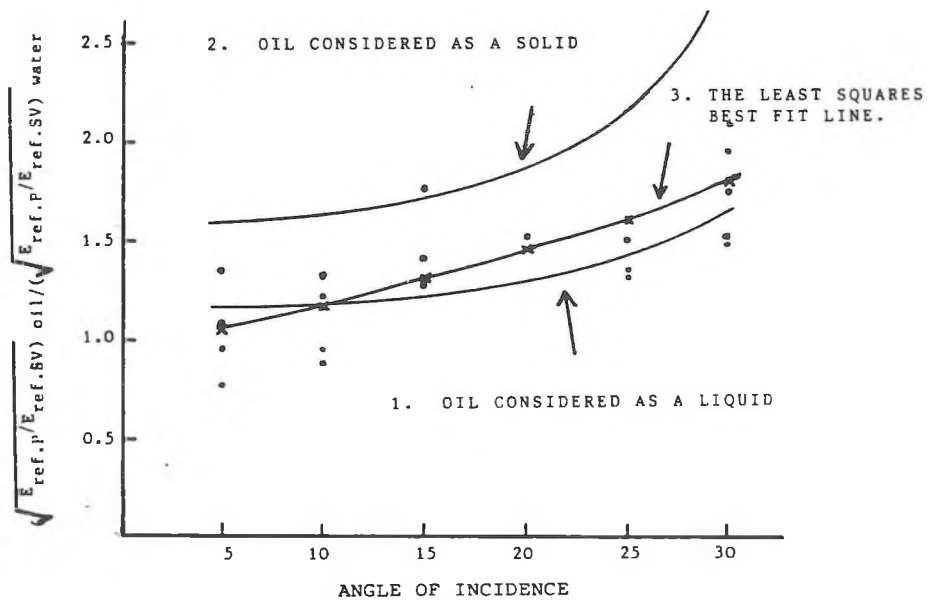


Figure 7  
P wave incident in the sea ice against oil or water. The ratio of the square root of the energy ratio of the reflected P wave to the reflected sv wave of ice/oil interface to ice/water interface vs. incident angle. ●: Experimental Data.

half of the oil "soaked" into the ice, leaving about 1 cm or less in contact with the ice surface at the end of the experiments. It was essential, of course, that air should not be trapped under the ice, and to this end the divers who assisted the experiments used closed circulation breathing apparatus and took every care to avoid such problems. A final detail concerns the pulse broadening of the shear wave. The broadening arises for reasons of geometry and the difference in the velocity of propagation between the compressional and shear waves. The principle effect it produces, in practice, is to reduce the signal amplitude. As the effect is the same for oil or water in contact with the ice, it would not appear at first sight to affect the ratios presented in the results.

When the oil measurements were completed, a piece of ice was removed from an area close to the site of the experiments (see Figure 4b). This piece was used for making measurements of the compressional and shear velocities of sound. The shear waves were produced by mode conversion at a prismatic face inclined at an angle of incidence; this face can be seen in the photograph with transducers mounted for shear velocity measurements.

Finally, several holes were bored at the test site to confirm the presence of the oil and its positioning (which had been placed originally by reference to markers pushed through the ice).

The data which had been collected was used to plot the graph shown in Figure 7. Clearly, at angles of  $\theta$  greater than  $10^\circ$ , there is little difficulty in saying that the experimental results indicate the presence of oil. It is interesting to note that the least squares best fit line gives an approximate fit to the visco-elastic properties which would be expected for the oil which was used. At angles of incidence of  $10^\circ$  and less, the indication of the presence of oil is uncertain. It is possible that the difficulty arises primarily from the path length of the shear wave. When the path length is shorter, the arrival of the slower wave is coincidental with the arrival of components of the compressional wave which have been scattered from relatively distant points in the ice sheet. As the time of flight of shear wave increases, this overlap decreases until it becomes relatively insignificant. The masking effect of these scattered signals causes the indicated amplitude of the shear wave to decrease because the compressional component is absent. If this is the case, the ratio plotted in Figure 7 will increase (i.e. when the compressional component is absent).

#### Design of Prototype Apparatus

Figure 8 shows the layout of the arrangement of the data acquisition and data processing for a prototype apparatus. The electronic part consists of a LeCroy instrument package in a Camac mini crate and an IBM-PC. The LeCroy instrument package consists of the following components housed in a Camac (IEEE-588) crate: (i) amplifier, (ii) digitizer, (iii) Camac to GPIB Interface, which allows the computer access to the Camac bus to program and receive data from the digitizer. Conventional techniques will be used in the probability assessment for the recognition of scattering from a rough lower surface of the ice.

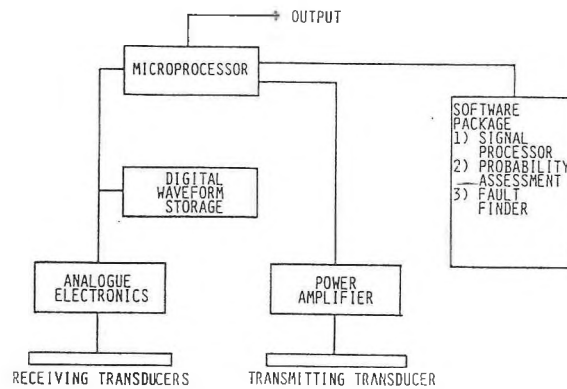


Figure 8  
Schematic for  
Prototype Apparatus

## CONCLUSION

The principles and experimental work of an acoustical method for detecting oil spill under salt ice are described. It is shown that initial field data support the method which is proposed and that quite thin layers of oil can be detected. Experimental results are supported by a fairly detailed statement of the theory involved. An outline design of a prototype apparatus is presented and future field trials on arctic sea ice will undoubtedly lead to modification of the ideas which are outlined here.

## ACKNOWLEDGEMENTS

This work is supported by funding from Esso Resources Canada Limited and the Environmental Protection Service.

## REFERENCES

1. Jones, H.W. and Kwan, H.W., "The Detection of Oil Spills Under Arctic Ice by Ultrasound", Proc. Fifth AMOP Technical Seminar, pp. 391-411, (1982).
2. Jones, H.W. and Kwan, H.W., "The Detection of Crude Oil Under Seawater in the Arctic Ocean", Proc. Sixth AMOP Technical Seminar, pp. 241-252, (1983).
3. Jones, H.W. and Kwan, H.W., "An Ultrasonic Exploration Technique for Finding Oil Under Arctic Sea Ice", Ultrasonics International 83 Conference Proceedings, pp. 182-187, (1983).
4. Mott, G., "Reflection and Refraction Coefficients at a Fluid/Solid Interface", J. Acoust. Soc. Amer., 50, (3), pp. 819-829, (1970).
5. Cooper, H.F., "Reflection and Transmission of Oblique Plane Waves at a Plane Interface Between Visco-elastic Media", J. Acoust. Soc. Amer., 42, (5), pp. 1064-1069, (1967).
6. Barlow, A.J. and Lamb, B.J., "The Visco-elastic Behaviour of Lubricating Oils under Cyclic Shearing Stress", Proc. Roy. Soc. A., 253, pp. 52-69, (1959).
7. Brekhovskikh, L.M., Waves in Layered Media, 2nd Ed. Academic Press, (1980).

# ICP QUARTZ SENSORS

(integrated circuit - piezoelectric)



MEASURAND	PRESSURE			FORCE			MOTION			
Model No.	102A05 112A21	101A02 111A22	108A 109A	200B Impact	201A03 221A03	208A05	302A	303A02	308B	
Range	psi, lb, g	100	15 000	80 000	10	50	500	500	50	
Resolution	psi, lb, g	0.004	0.2	2	0.0004	0.02	0.2	0.02	0.002	
Sensitivity	mV/unit	50	1	0.1	500	10	1	10	100	
Resonant Frequency	Hz	250 000	400 000	300 000	70 000	70 000	70 000	45 000	70 000	25 000
Output Voltage	V	5	5	8	5	5	5	5	5	
Temperature Range	°F	-100 to +275	-100 to +275	-100 to +275	-100 to +250	-100 to +250	-100 to +250	-100 to +250	-40 to +200	-100 to +250
Vibration (max.)	g	2000	2000	2000	2000	2000	2000	2000	1000	500
Size (dia. x length)	in	.248 x 1.38	.248 x 1.38	.320 x 1.70	.650 x 1.15	.650 x 1.15	.625 x 1.025	.484 x 1.30	.275 x .58	.75 x 1.32
Weight	gram	6	6	12	14	14	25	25	3	87
Connector (coaxial)		10-32	10-32	10-32	10-32	10-32	10-32	5-44	10-32	
Other Models (includes numerous other ranges, sizes and sensitivities)	Blast Cryogenic Helium Bleed Water Cooled	Spark Plug Sound Conformal Hi-Frequency	Other Ranges Other Sizes Miniature Impact	Press Monitor Industrial Ring & Link Sledge Hammers	Seismic Hi-Sensitivity Ring Industrial	Hermetic Gnd. Isolated				

**ICP QUARTZ SENSORS** with built-in microelectronic amplifiers simplify the task of dynamic measurements. You can operate them over long coaxial or two wire cables, couple directly to your scope or analyzer and cover extremely wide ranges with just one sensor. You'll also appreciate their value, economy, ruggedness, reliability and stability. They are structured with crystalline quartz, stress-gage elements and function to transfer dynamic phenomena into electrical signals, more convenient for recording or analyzing.

**OTHER PRODUCTS** include a complete line of conventional charge-mode transducers and associated charge amplifiers. Piezoelectronic products include power units, voltage amplifiers, filters, integrators, vibration meters, and digital peak meters. Instrumented impulse hammers help test the behavior of structures. Dynamic calibrators build confidence in quartz sensors. These precision, space-age products are all made in the U.S.A. by the No. 1 American quartz company. For more information, just call or write.

PCB PIEZOTRONICS, INC.  
3425 Walden Avenue, Depew, New York 14043-2495  
Telephone: 716-684-0001, TWX: 710-263-1371

**PCB**  
PIEZOTRONICS

*"Leader in Quartz Dynamic Instrumentation"*

# **Manager Electro Acoustic Design/Development**

---

Northern Telecom is a world leader in the advanced technology of telecommunications. Our leadership in virtually every aspect of design, manufacture and marketing is a direct result of a special environment that we have created that encourages both people and technological innovation to flourish.

Based in our Station Apparatus Division in London, you will provide guidance to a technical staff of engineers and technologists involved in the development and support of telephony products. In addition you will be responsible for electro acoustic device (loudspeakers, microphones, earphones) design and system evaluation including measurements.

You will have at least 5 years industry experience and a familiarity with acoustic standards i.e., IEEE, IEC and CCITT. Background in analog electronics and telephony would be strong assets. A Bachelors degree in electrical or electronic engineering is mandatory.

As well as receiving first-class remuneration, you will be provided with outstanding scope for both personal and professional growth.

Please send your detailed resume, in confidence, to:

**Larry Zalmers  
Senior Specialist, Human Resources  
Station Apparatus Division  
Northern Telecom Canada Ltd.  
Sise Road, P.O. Box 5155  
London, Ontario N6A 4N3**



**We hire talent**

**nt** northern  
telecom

**2nd INTERNATIONAL CONGRESS ON ACOUSTIC INTENSITY**

Senlis (near Paris), France  
23-26 September 1985

Papers, to be presented in French or English (with simultaneous translation), will cover the following areas: general concepts of vector fields, recent developments in instrumentation, localisation and characterization of sound sources, sound power determination, transmission loss and absorption of panels, energy propagation in fluids and structures, standardisation.

Proceedings of the congress will be available at the congress. Further information can be obtained from:

Dr. M. Bockhoff  
CETIM  
B.P. 67  
F-60304 Senlis  
France  
Tel.: (33) (4) 453.32.66  
Telex: 140006F

**FIRST SOUTH AFRICAN CONGRESS ON ACOUSTICS**

To celebrate its tenth anniversary, The South African Acoustics Institute (SAAI) is organizing the First South African Congress on Acoustics which will be held at the CSIR Conference Centre, Meiring Naudé Road, Pretoria, from 2-4 October 1985. Contact:

Symposium Secretariat  
S.379, CSIR  
P.O. Box 395  
Pretoria 0001, South Africa

**CALENDAR 1985**

6-10 April 1985  
Man Under Vibration  
Moscow, USSR

15-17 April 1985  
Institute of Acoustics Spring Conference  
York, England

22-26 April 1985  
International Symposium on Acoustical Imaging  
The Hague, The Netherlands

3-6 May 1985  
78th Audio Engineering Society Convention  
Anaheim, California, U.S.A.

6-8 May 1985  
International Symposium on Hand-Arm Vibrations  
Helsinki, Finland

29-31 May 1985  
GALF Speech Group Meeting  
Paris, France

3-5 June 1985  
NOISE CON 85  
Ohio State University  
Columbus, OH, U.S.A.

2-4 July 1985  
Ultrasonics International '85  
Kings College, London, UK

3-5 July 1985  
IUTAM Symposium on Aero and Hydroacoustics  
Lyon, France

4-8 August 1985  
Photoacoustic, Thermal and Related Sciences  
Ecole Polytechnique, Montreal, Quebec

4-9 August 1985  
International Congress on Education of the Deaf  
Manchester, England

27-29 August 1985  
5th FASE  
Thessaloniki, Greece

18-20 September 1985  
INTER-NOISE 85  
Munich, West Germany

23-26 September 1985  
2nd International Congress on Acoustic  
Intensity  
Senlis, France

30 September - 4 October 1985  
Canadian Acoustical Association  
Symposium  
Ottawa, Canada

1-4 October 1985  
Architectural Acoustics  
Strbske Pleso, Czechoslovakia

13-17 October 1985  
79th Audio Engineering Society  
Convention  
New York, NY, U.S.A.

23-25 October 1985  
International Conference on Speech  
Technology  
Brighton, UK

4-8 November 1985  
Fall Meeting of Acoustical Society of  
America  
Nashville, TN, U.S.A.

#### SUSTAINING MEMBERS UPDATE

Due to the costs of typesetting the list of sustaining members on the rear covers, new sustaining members will only be added once each year in the July issue. Additional sustaining members are listed below.

Acoustec Inc.  
Conseillers en Acoustique et  
Controle du Bruit  
106 Chaudière  
St. Nicolas, Quebec G0S 2Z0  
Tel.: (418) 839-0101

Canada Post Corporation

McCarthy Robinson Inc.  
"Matrix Industrial Silencers"  
321 Progress Avenue  
Scarborough, Ontario M1P 2Z7  
Tel.: (416) 298-1630

#### ACTIVITY INVOLVING ACOUSTICS IN CANADIAN STANDARDS ASSOCIATION

Published CSA Standards (Committee Z107: Acoustics and Noise Control)

Designation	Title	Status (and Price)
Z107.0	Definitions of Common Acoustical Terms Used in CSA Standards	Issued 1984 (\$12.00)
Z107.4	Pure Tone Conduction Audiometers For Hearing Conservation and For Screening	Issued 1975 (\$5.00) Revisions approved by committee New edition expected in 1985
Z107.21	Procedure For Measurement of the Maximum Exterior Sound Level of Pleasure Motor Boats	Issued 1977 (\$8.00) Subcommittee review in progress

Z107.22	Procedure For Measurement of the Maximum Exterior Sound Level of Stationary Trucks With Governed Diesel Engines	Issued 1977 Subcommittee review in progress	(\$8.00)
Z107.23	Procedure For Measurement of the Maximum Interior Sound Level in Trucks With Governed Diesel Engines	Issued 1977 Subcommittee review in progress	(\$7.75)
Z107.24	Procedure For Measurement of the Exterior Sound Level of Railbound Vehicles	Approved by CSA Z107 committee Publication expected 1985	
Z107.25	Procedure For Measurement of the Exhaust Sound Level of Stationary Motorcycles	Issued 1983	(\$8.75)
Z107.31	Test Procedure For Measurement of Sound Levels From Agricultural Machines	Subcommittee review in progress	
Z107.32	Test Procedure For Measurement of Sound Emitted From Construction, Forestry and Mining Machines to the Operator Station and Exterior of the Machine	Approved by CSA Z107 committee Publication expected 1985	
Z107.51	Procedure For In-Situ Measurement of Noise From Industrial Equipment	Issued 1980 Subcommittee review in progress	(\$11.00)
Z107.52	Recommended Practice For the Prediction of Sound Pressure Levels in Large Rooms Containing Sound Sources	Issued 1983	(\$17.00)
Z107.53	Procedure For Performing a Survey of Sound Due to Industrial, Institutional or Commercial Activities Sources	Issued 1982	(\$10.00)
Z107.54	Procedure for Measurement of Sound and Vibration due to Blasting Operations	Committee ballot and resolution of comments in progress	
Z107.55	Recommended Practice for the Prediction of Sound Levels Received at a Distance from an Industrial Plant	Committee ballot and resolution of comments in progress	

Handling and mailing charges are additional. Copies may be ordered or obtained from CSA offices in Moncton (855-5596), Montreal (694-8111), Toronto (747-4000), Winnipeg (632-6633), Edmonton (436-8553), or Vancouver (273-4581). The mailing address for CSA Head Office is 178 Rexdale Blvd., Toronto, Ontario, M9W 1R3. Technical enquiries concerning standards in the Z107 series may be addressed to J.D. Quirt, Division of Building Research, National Research Council of Canada, Ottawa, K1A 0R6 (telephone: (613) 993-2305).

Other CSA Standards with Acoustical Content

---

CAN3-Z62.1-R1984	Chain Saws (National Standard for Product Certification)
Z94.2-R1983	Hearing Protectors
C22.2 No. 0.7-M1984	Equipment Electrically Connected to a Telecommunication Network (Specifies maximum sound from telephones)

Foreign Standards Endorsed by CSA Committee Z107 for Use in Canada

---

(Extensive revision and expansion of this list is expected in 1985)

ANSI/ASTM C384-77	Impedance and Absorption of Acoustical Materials by the Impedance Tube Method
ANSI/ASTM C423-1977	Sound Absorption and Sound Absorption Coefficients by the Reverberation Room Method
ANSI/ASTM E336-1977	Measurement of Airborne Sound Insulation in Buildings
ANSI/ASTM E492-1977	Laboratory Measurement of Impact Sound Transmission Through Floor-Ceiling Assemblies Using the Tapping Machine
ANSI S1.4-1983	Specification for Sound Level Meters
ANSI S1.13-1971(R1976)	Methods for the Measurement of Sound Pressure Levels
ANSI S1.11-1966(R1976)	Octave, Half-Octave, and Third-Octave Band Filter Sets Sound Level Meters
ASTM E90-1981	Laboratory Measurements of Airborne Sound Transmission Loss of Building Partitions
ANSI S1.31-1980	Precision Methods for the Determination of Sound Power Levels of Broad-Band Noise Sources in Reverberation Rooms
ANSI S1.32-1980	Precision Methods for the Determination of Sound Power Levels of Discrete Frequency and Narrow-Band Noise Sources in Reverberation Rooms

New CSA Standards Under Development by Committee Z107

---

P9.2.18	Noise Monitoring around Industrial Complexes	Writing group preparing draft
P9.2.22	Procedure for the Measurement of Occupational Noise Exposure	Subcommittee review in progress
P9.2.99	Pure Tone Air Conduction Threshold Audiometry for Hearing Conservation Purposes	Writing group preparing draft

# The Canadian Acoustical Association l'Association Canadienne de l'Acoustique



## President/*Président*

C.W. Sherry  
Research Centre  
P.O. Box 300  
Senneville, Quebec H9X 3L7

(514) 457-6810

## Past President/*Ancien Président*

T.D. Northwood  
140 Blenheim Drive  
Ottawa, Ontario K1L 5B5

(613) 746-1923

## Secretary/*Secrétaire*

D.A. Benwell  
Environmental Health Centre, R.P.B.  
Health and Welfare Canada  
Room 233, Tunney's Pasture  
Ottawa, Ontario K1A 0L2

(613) 990-8892

## Treasurer/*Trésorier*

T. Ho  
Bruel & Kjaer Canada Ltd.  
5520 Minoru Blvd. Room 202  
Richmond, B.C. V6X 2A9

(604) 278-4257

## Directors/*Directeurs*

S. Abel, L. Cuddy, R. Héту, J. Leggat, J. Nicolas, D. Quirt, L.T. Russel, P. Vermeulen

## 12 ICA COMMITTEE CHAIRMEN



E.A.G. Shaw	Executive Committee	(613) 993-2840
S.M. Abel	Local Planning Committee	(416) 596-3014
J.A. Ayres	Finance Committee	(416) 274-3224
A.T. Edwards	Congress Facilities	(416) 845-1840
T.F.W. Embleton	Technical Programme Committee	(613) 993-2840
J.R. Hemingway	Exhibition Committee	(416) 793-0409
R.B. Johnston	Support Committee	(416) 845-8900
J. Manuel	Secretariat Committee	(416) 965-4120
J.E. Piercy	Committee on Coordinated Meetings	(613) 993-2840
A.C.C. Warnock	Congress Advisory Committee	(613) 993-2305

# SUSTAINING SUBSCRIBERS/ABONNES DE SOUTIEN

The Canadian Acoustical Association gratefully acknowledges the financial assistance of the Sustaining Subscribers listed below. Annual donations (of \$95.00 or more) enable the journal to be distributed to all at a reasonable cost. Sustaining Subscribers receive the journal free of charge. Please address donation (made payable to the Canadian Acoustical Association) to the Associate Editor-Advertising.

*L'Association Canadienne de l'acoustique tient à témoigner sa reconnaissance à l'égard de ses Abonnés de Soutien en publiant ci-dessous leur nom et leur adresse. En amortissant les coûts de publication et de distribution, les dons annuels (\$95.00 et plus) rendent le journal accessible à tous nos membres. Des Abonnés de Soutien reçoivent le journal gratis. Pour devenir un Abonné de Soutien, faites parvenir vos dons (chèque ou mandat de poste fait au nom de l'Association Canadienne de l'Acoustique) au membre de la Rédaction en charge de la publicité.*

**John R. Bain Associates Limited**  
Consultants in Acoustics  
Mississauga, Ontario L4X 2C7  
Tel.: (416) 625-4773

**Barman Coulter Swallow Associates**  
Engineers in Acoustics & Vibration  
1 Greensboro Drive  
Rexdale, Ontario M9W 1C8  
Tel.: (416) 245-7501

**Barron & Associates**  
Consulting Acoustical Engineers  
Noise, Vibration, Audio/Video  
Vancouver, British Columbia  
Tel.: (604) 872-2508

**H.L. Blachford Limited**  
Noise Control Products  
Engineering/Manufacturing  
Mississauga: Tel.: (416) 823-3200  
Montreal: Tel.: (514) 866-9775  
Vancouver: Tel.: (604) 263-1561

**William Bradley & Associates**  
Consulting Acoustical Engineers  
Ingénieurs conseils en acoustique  
Montréal, Québec H3V 1C2  
Tel.: (514) 735-3846

**BVA Manufacturing Limited**  
Noise Control Products  
2215 Midland Avenue  
Scarborough, Ontario M1P 3E7  
Tel.: (416) 291-7371

**CA Engineering Services**  
P.O. Box 2520, DEPS  
Dartmouth, Nova Scotia B2W 4A5

**Eckel Industries of Canada Limited**  
Noise Control Products  
Audiometric Rooms - Anechoic Chambers  
Morrisburg, Ontario K0C 1X0  
Tel.: (613) 543-2967

**Electro Medical Instrument Company**  
Audiometric Rooms and Equipment  
359 Davis Road  
Oakville, Ontario L6J 5E8  
Tel.: (416) 845-8900

**Bruel & Kjaer Canada Limited**  
90 Leacock Road  
Pointe Claire, Québec H9R 1H1

**Higgot-Kane Industrial Noise Control Limited**  
1085 Bellamy Road North  
Suite 214  
Scarborough, Ontario M1H 3C7  
Tel.: (416) 431-0641

**Hooker Noise Control Inc.**  
360 Enford Road  
Richmond Hill, Ontario L4C 3E8

**Marshall Macklin Monaghan Ltd.**  
Consulting Engineers  
275 Duncan Mill Road  
Don Mills, Ontario M3B 2Y1  
Tel.: (416) 449-2500

**Nelson Industries Inc.**  
Corporate Research Department  
P.O. Box 428  
Stoughton, WI 53589  
U.S.A.

**SNC Inc.**  
Environment Division  
Noise and Vibration Control  
Contrôle du bruit et des vibrations  
1, Complexe Desjardins  
Montréal, Québec H5B 1C8  
Tél.: (514) 282-9551

**SPAARG Engineering Limited**  
Noise and Vibration Analysis  
Windsor, Ontario N9B 1N9  
Tel.: (519) 254-8527

**Tacet Engineering Limited**  
Consultants in Vibration and Acoustical Design  
111 Ava Road  
Toronto, Ontario M6C 1W2  
Tel.: (416) 782-0298

**Valcoustics Canada Limited**  
Suite 502  
30 Drewry Avenue  
Willowdale, Ontario M2M 4C4

**R.B. Johnston**  
349 Davis Road  
Oakville, Ontario L6J 5E8

**E.H. Bolstad**  
P.O. Box 5768, Station "L"  
Edmonton, Alberta T6C 4G2